Development of Hydrogel-based Bioinks Consisting of K-carrageenan/Methylcellulose and Pluronic F127/Methylcellulose

Wannisa Boonlai

A Thesis Submitted in Fulfillment of the Requirements for the
Degree of Doctor of Philosophy in Pharmaceutical Sciences
Prince of Songkla University
2022

Development of Hydrogel-based Bioinks Consisting of K-carrageenan/Methylcellulose and Pluronic F127/Methylcellulose

Wannisa Boonlai

A Thesis Submitted in Fulfillment of the Requirements for the
Degree of Doctor of Philosophy in Pharmaceutical Sciences
Prince of Songkla University
2022

Thesis Title Development of Hydrogel-based Bioinks Consisting of K-carrageenan/Methylcellulose and Pluronic F127/Methylcellulose

Author Miss Wannisa Boonlai

Major Program Pharmaceutical Sciences

Major Advisor

.....

(Prof. Dr. Vimon Tantishaiyakul)

Co-advisor

.....

(Assoc. Prof. Dr. Namon Hirun)

Examining Committee:

.....Chairperson

(Assoc. Prof. Dr. Satit Puttipipatkhachorn)

.....Committee

(Prof. Dr. Damrongsak Faroongsarng)

.....Committee

(Prof. Dr. Ruedeekorn Wiwattanapatapee)

.....Committee

(Prof. Dr. Vimon Tantishaiyakul)

.....Committee

(Assoc. Prof. Dr. Namon Hirun)

The Graduate School, Prince of Songkla University, has approved this thesis as fulfillment of the requirements for the Doctor of Philosophy Degree in Pharmaceutical Sciences

.....

(Prof. Dr. Damrongsak Faroongsarng)

Dean of Graduate School

This is to certify that the work here submitted is the result of the candidate's own investigations. Due acknowledgement has been made of any assistance received.

.....Signature
(Prof. Dr. Vimon Tantishaiyakul)
Major Advisor

.....Signature
(Assoc. Prof. Dr. Namon Hirun)
Co-advisor

.....Signature
(Miss Wannisa Boonlai)
Candidate

I hereby certify that this work has not been accepted in substance for any degree, and is not being currently submitted in candidature for any degree.

.....Signature

(Miss Wannisa Boonlai)

Candidate

ชื่อวิทยานิพนธ์ การพัฒนาหมึกพิมพ์ชีวภาพจากไฮโดรเจลที่ประกอบด้วยเค-คาราจีแนน/เมทิลเซลลูโลสและพลูโรนิก F127/เมทิลเซลลูโลส
ผู้เขียน นางสาววรรณนิสา บุญไหล
สาขาวิชา เภสัชศาสตร์
ปีการศึกษา 2564

บทคัดย่อ

ในงานวิจัยนี้พัฒนาหมึกพิมพ์ชีวภาพ 2 ระบบ คือ ระบบที่ 1 หมึกพิมพ์ชีวภาพที่ผสมระหว่างแคปป้า-คาราจีแนน (KC) และเมทิลเซลลูโลส (MC) (KC/MC) และระบบที่ 2 คือ พลูโรนิค F127 (PF)/ เมทิลเซลลูโลส (PF/MC) ซึ่งพบว่า หมึกพิมพ์ชีวภาพที่ศึกษาสามารถประยุกต์ใช้ในการพิมพ์แบบสามมิติ สารผสมระหว่าง KC และ MC ทดสอบด้วยการการพิมพ์ชีวภาพแบบ extrusion-based โดยเติม KCl ความเข้มข้น 0.1% w/w (0.1KCl) เป็น ionic crosslinking เพื่อเพิ่มคุณสมบัติทางกายภาพของไฮโดรเจล KC (0.3%w/w) MC (7%w/w) (0.3KC/7MC) นอกจากนี้ยังใช้เซลลูโลสนาโนคริสตัล (CNC) ความเข้มข้นต่างๆ ผสมกับไฮโดรเจล 0.3KC/0.1KCl/7MC เพื่อเพิ่มประสิทธิภาพเชิงกล shear thinning และ คุณสมบัติ thixotropic ซึ่งมีความสำคัญสำหรับการพิมพ์ชีวภาพแบบ extrusion-based โดยการเติม CNC ความเข้มข้น 2 %w/w (2CNC) และ 4% w/w (4CNC) ในไฮโดรเจล (0.3KC/0.1KCl/7MC/2CNC และ 0.3KC/0.1KCl/7MC/4CNC) แสดงพฤติกรรมแบบ thixotropic ที่ดี ซึ่งการเพิ่มความเข้มข้นของ CNC ยังแสดงให้เห็นพฤติกรรม shear-thinning ที่มากขึ้นอีกด้วย รวมถึง compressive stress มีค่าสูงขึ้นอย่างมีนัยสำคัญเมื่อเติม CNC และเซลล์สามารถเติบโตได้ดี (> 90%) นอกจากนี้หมึกพิมพ์ชีวภาพอีกระบบ คือ PF/MC ที่ผสมระหว่าง PF ความเข้มข้น 18% (w/w) กับ MC ความเข้มข้น 4% (w/w) (18PF/4MC) และ PF ความเข้มข้น 20% (w/w) กับ MC ความเข้มข้น 4% (w/w) (20PF/4MC) แสดงพฤติกรรม thixotropic ที่ดี โดยที่ความเข้มข้นของ PF สูง คือ 20PF/MC พบว่ามี shear-thinning ที่ดีกว่า 18PF/MC อย่างไรก็ตาม 20PF/4MC สามารถพิมพ์ได้ดีกว่า 18PF/4MC เล็กน้อย สำหรับ compressive stress จะขึ้นอยู่กับความเข้มข้นของ PF โดยแสดงความสัมพันธ์ระหว่าง compressive stress กับ strain (20PF/4MC > 18PF/4MC) นอกจากนี้ เซลล์สามารถเติบโตได้ดี (> 90%) เมื่อผสมกับ 20PF/4MC และ 18PF/4MC ดังนั้น ไฮโดรเจล 0.3KC/0.1KCl/7MC/4CNC และ 20PF/4MC จึงมีคุณสมบัติที่ดีสำหรับการพิมพ์ชีวภาพแบบ 3 มิติ

Thesis Title Development of Hydrogel-based Bioinks Consisting of K-carrageenan/Methylcellulose and Pluronic F127/Methylcellulose
Author Miss Wannisa Boonlai
Major Program Pharmaceutical Sciences
Academic Year 2021

ABSTRACT

K-carrageenan (KC)/methylcellulose (MC) (KC/MC) based hydrogels and Pluronic F127 (PF)/ MC (PF/MC) based hydrogels have shown promising results for three dimensional (3D) bioprinting applications. The blend of various KC and MC were investigated for extrusion-based bioprinting. Physical property of the 0.3%w/w KC/7 %w/w MC (0.3KC/7MC) hydrogels was successfully enhanced using ionic crosslinking with 0.1% w/w KCl (0.1KCl). Furthermore, various concentrations of cellulose nanocrystal (CNC) were incorporated into the 0.3KC/0.1KCl/7MC hydrogel to increase its mechanical performance. Shear thinning and thixotropic properties are important for extrusion-based bioprinting. The presence of 2 %w/w CNC (2CNC) and 4% w/w CNC (4CNC) in the hydrogels (0.3KC/0.1KCl/7MC/2CNC and 0.3KC/0.1KCl/7MC/4CNC) exhibited good thixotropic behavior. In addition, increasing CNC concentration showed greater shear thinning behavior. A good cell viability (> 90%) was obtained for the 3D bioprinted 0.3KC/0.1KCl/7MC/2CNC and 0.3KC/0.1KCl/7MC/4CNC constructs. Furthermore PF/MC system, the blends of 18% (w/w) PF/ 4% (w/w) MC (18PF/4MC) and 20% (w/w) PF/4% (w/w) MC (20PF/4MC) exhibited good thixotropic behavior. At high PF concentration of 20PF/MC showed better shear thinning behavior than 18PF/MC. The 20PF/4MC hydrogel exhibited better printability than 18PF/4MC. The compressive mechanical property was significantly higher in the presence of PF. In addition, the blend of 20PF/4MC and 18PF/4MC showed good cell viability (>90%).

The novel 0.3KC/0.1KCl/7MC/4CNC and 20PF/4MC hydrogel showed good attributes for a promising 3D bioprinting material.

ACKNOWLEDGEMENT

I would like to express my deepest appreciation and gratitude to my advisor Professor Dr. Vimon Tantishaiyakul for her inspiring guidance, encouragement and support everything throughout this work.

I would like to thank Associate Professor Dr. Namon Hirun my co-advisor for helpful advice in this thesis work.

I would like to thank Associate Professor Dr. Satit Puttipipatkhachorn, Professor Dr. Damrongsak Faroongsarng and Professor Dr. Ruedeekorn Wiwattanapatapee for serving on my supervisory committee. I am deeply grateful.

I also wish to thank the Department of Pharmaceutical Chemistry, Prince of Songkla University, Medical Science Research and Innovation Institute, Prince of Songkla University, Scientific Instrument and Testing, Prince of Songkla University and School of Pharmacy Walailak University for their kindness and support for using equipment.

Finally, I would also like to thank my parents and friends. I wish thank them for the understanding during all of the times and their steady love that supports me.

Wannisa Boonlai

CONTENTS

CONTENTS (CONTINUED)

CONTENTS (CONTINUED)

LIST OF TABLES

LIST OF FIGURES

LIST OF FIGURES (CONTINUED)

LIST OF FIGURES (CONTINUED)

Figures **Page**

LIST OF ABBREVIATIONS AND SYMBOLS

KC	=	K-carrageenan
MC	=	Methylcellulose
CNC	=	Cellulose nanocrystal
PF	=	Pluronic F127
KCl	=	Potassium Chloride
EMEM	=	Eagle's Minimum Essential Medium
DMSO	=	Dimethyl sulfoxide
PBS	=	Phosphate buffered saline
DPBS	=	Modified without calcium chloride and magnesium chloride
SEM	=	Scanning Electron Microscope
g	=	Gram
mL	=	Milliliter
µl	=	Microliter
mg	=	Milligram
min	=	Minute
w/w	=	Weight per weight
Hz	=	Hertz
SD	=	Standard deviation
mm	=	Millimeter
cm^{-1}	=	Reciprocal centimeter
nm.	=	Nanometer
min	=	Minute
h	=	Hour
mm	=	Millimeter
s	=	Second
N	=	Newton
kPa	=	Kilopascal

LIST OF ABBREVIATIONS AND SYMBOLS (CONTINUED)

G′	=	Storage modulus
G″	=	Loss modulus
%	=	Percent
°C	=	Degree of celcius
η	=	viscosity
$\dot{\gamma}$	=	shear rate
K	=	consistency index
n	=	flow index
W_r	=	Relative percentage of degradation
W_0	=	Weights of a hydrogel sample before soaking
W_1	=	Weights of a hydrogel sample after soaking

CHAPTER 1

INTRODUCTION

1.1 Background and Rationales

Three-dimensional (3D) bioprinting is an emerging technology that combines 3D printing and biotechnology. Therefore, the bioengineered scaffold should provide several factors such as biocompatibility, biodegradability, and physical properties (1). Recently, bioprinting gets more and more attention due to its use in tissue engineering (2, 3). Bioprinting is focused more on the deposition of biological materials such as living cells or tissues into 3D structures (3). For bioprinting, commercial printing ink was replaced with a bio-printing ink, or a bio-ink. With the hope of solving the shortage of transplantable organ, 3D bioprinting is particularly attractive due to its potential in fabricating artificial tissues or organs through layer-by-layer stacking of biomaterials and cells (4). Synthetic polymers provide various benefits including high mechanical properties, controllable degradation and reproducibility. However, lack of biological signals is a significant limitation of synthetic polymers (5). On the other hand, natural polymers provide good biological features but their insufficient mechanical property is recognized as one of disadvantages (6). To use these natural polymers as bioinks for 3D bioprinting, the hybrid, composite or blend of these polymers have been investigated such as alginate/ gelatin chitosan/ gelatin, gelatin/fibrinogen and gelatin methacrylate (7-10). Nevertheless, there are also some limitations such as poor cellular adhesion, limiting cell proliferation and differentiation. Moreover, factors including types of polymer, molecular weights, concentrations and compositions have significant effects on gelation, viscosity, mechanical strength and network properties reflecting printing fidelity and cell viability and proliferation (11).

Bioinks are the most materials for bioprint. The bioink mostly used for 3D plotting for support structures. Hydrogel are three dimensional polymeric networks that have a high water content, biocompatibility and low cytotoxicity (12). The

hydrogel bioink used as cell carrier, cell viability, printability and mechanical strength of printed scaffolds (13). In addition, hydrogels allow cell encapsulation in a highly hydrated mechanically supportive 3-dimensional environment and also allow for efficient and homogeneous cell seeding (14). Moreover, most hydrogels are biocompatible and can be utilized as bioinks. Therefore, hydrogels are significant candidates for bioprinting. The important features of hydrogels for bioprinting include printability and mechanical properties. For printability, hydrogels should have suitable viscosity and shear-thinning property of which viscosity decrease as the shear rate increases (15-17). Also, for good printability of highly viscous hydrogels with an extrusion-based bioprinter, thixotropic property of the gels (the viscosity at a given flow condition decrease over time) is required (15, 18). Besides printability, the printed materials should have suitable mechanical strength to support the 3D structure (19). Moreover, living cells must be deposited in the printed constructs while printing without critically affecting the cells viability (20). So far, various hydrogels including collagen, gelatin, alginate, hyaluronic acid and pluronic have been demonstrated their use in extrusion-based bioprinting. Nevertheless, these hydrogel-based bioinks have not been able to fulfill the requirements for bioprinting due to their limited printability, inferior mechanical properties, slow gelation or insufficient cytocompatibility when used alone (21-23). Due to limitations of these single-component hydrogels, hybrid hydrogels and physical blending hydrogels have been investigated for extrusion-based bioprinting (24, 25).

Pluronic F127 (PF), a triblock copolymer, can form gel at concentration of ≥15% w/w. Although PF has been used for the *in-situ* drug delivery of various drugs and explored for tissue engineering, there are certain issues of concern such as mechanical strength as well as their stability due to its delicate network. In addition, high concentration of PF is cytotoxic. Recently, we have developed hydrogels consisting of PF and methylcellulose (MC) for etidronate delivery and their application for osteogenesis (26). The blend of PF/MC showed good cytocompatiblity; and viability of MC3T3-E1 and C2C12 cells in the presence PF was significantly increased in the presence of MC. It has been found that MC can protect the cells from a physical stress (27). We also found that the blends of PF/MC are thermoreversible and form gel at

body temperature (26). Therefore, we are interested in developing a suitable bioink from PF127/MC by varying ratio and concentration of both materials or addition of suitable salts that can modify gel properties (28).

Besides PF/MC, K-carrageenan (KC) is a sulphated polysaccharide extracted from red seaweed (29). KC can form thermoreversible gels. At high temperature (above 60°c) can be easily dissolved in water, presenting a random coil structure. During the cooling, the macromolecules interact forming a brittle gel, presenting a double helixes coil followed by the aggregation of helices (30). MC is a water-soluble cellulose polysaccharide derivatives; MC has inverse thermal gelling properties. At low temperature, MC can dissolve in water to form solution (30-50 °C). However, at high temperature, hydrogen bonds are broken and hydrophobic junction form to produce a gel (above 50 °C) (31). Therefore, it is interesting to improve the properties of MC-based hydrogel as bioink by combining with KC and/or other polymers

In this study, attention was paid to blend of KC/MC and PF/MC. Which can modify viscosity of the hydrogel will be able to produce a suitable bioink to support cell differentiation for the bioprinting 3D scaffolds.

1.2 Objectives of the research

1.2.1 To develop hydrogel-based bioinks consisting of KC/MC and PF/MC
1.2.2 To evaluate printability of the hydrogels
1.2.3 To evaluate mechanical properties of the hydrogels
1.2.4 To evaluate cell viability of the bioprinted constructs

CHAPTER 2

LITERATURE REVIEW

2.1 Three-dimensional (3D) bioprinting

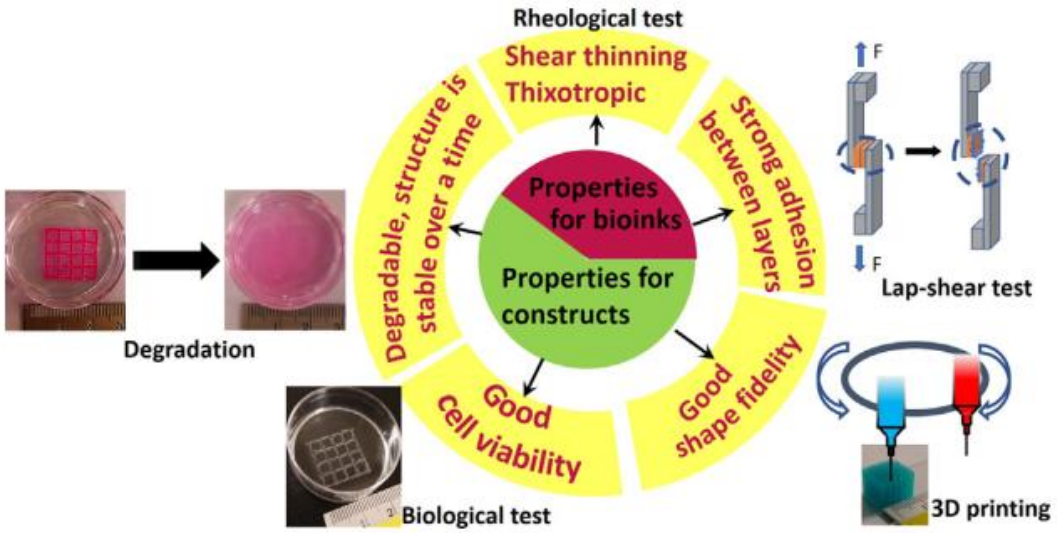

Figure 1. Properties of bioinks and constructs (32)

Three- dimensional (3D) bioprinting is an emerging technology that combines 3D printing and biotechnology. Although the concept of bioprinting was initiated more than 10 years ago, the current progress of bioprinting is still in its initial stage and far from industrial applications (33). Recently, bioprinting gets more and more attention due to its use in tissue engineering (3, 34). Bioprinting is focused more on the deposition of biological materials such as living cells or tissues into 3D structures (3). For bioprinting, commercial printing ink was replaced with a bio-printing ink, or a bioink. Generally, a promising tissue engineering approach involves the development of 'tissue scaffolds', which are 3-dimensional constructs comprised of biomaterials and cells to support and guide the regeneration of targeted tissues by facilitating the cell differentiation, migration, and proliferation (35). With the hope of solving the shortage

of transplantable organ, 3D bioprinting is particularly attractive due to its potential in fabricating artificial tissues or organs through layer-by-layer stacking of biomaterials and cells (4). Bioprinting also causes less danger of organ transplant rejection than traditional treatment of grafting (36). In addition, the properties of constructs and bioink such as mechanical property, rheological, biological and degradation of the materials, which are crucial for printing of complex and functional 3D structures (Figure 1).(32) Nowadays, various bioprinting methods have been developed. These include laser-based printing (37), inkjet-based printing (38), valve-based printing (39) and extrusion-based printing (40). Among these technologies, extrusion-based bioprinting is one of the most popularly methods due to its ease of operation and the capability to print a wide variety of bioinks with high cell densities (3, 15, 34).

2.2 Bioink

Bioink is a material that provide a supportive extracellular matrix environment and safeguard cells from the stresses a cell during printing. Hydrogels are 3D networks that have a high-water content. Hydrogels have been widely used as cell carriers and scaffolds in tissue engineering due to their structural similarities to the natural extracellular matrices. In addition, hydrogels allow cell encapsulation in a highly hydrated mechanically supportive 3-dimensional environment and also allow for efficient and homogeneous cell seeding (14). Moreover, most hydrogels are biocompatible and can be utilized as bioinks. The connection of the network within the polymeric hydrogel may be a covalent bonding, charge interaction, hydrogen bonding, hydrophobic interaction or van der Waals interaction (41). Composite hydrogels as bioinks have been developed, and a summary of composite bioinks for tissue engineering is shown in Table 2.1.

Table 2.1. A summary of composite bioinks for tissue engineering

Composite Bioink	Cells	3D Bioprinting Technique	Application	Reference
Alginate/gellan gum	Bovine chondrocytes	Extrusion	Tissue engineering and regenerative medicine in general	(42)
Alginate/polyvinyl alcohol	MC3T3-E1 (Mouse calvaria 3T3-E1)	Extrusion	Bone	(43)
Gelatin/alginate	Mouse chondrocytes	Extrusion	Cartilage	(44)
GelMA/KCA (Kappa-carrageenan)	MC3T3-E1 (Murine 3T3 preosteoblasts, Subclone 4)	Extrusion	Large human tissues, Bioactive 3D structures	(45)
Chitosan/alginate	MC3T3-E1	Extrusion	Bone	(46)
Alginate /methylcellulose	hTERTMSC	Extrusion	Bone, drug delivery	(47)
Pluronic-GelMA	HUVECs	Extrusion	Vasculature-like structures	(48)

Composite Bioink	Cells	3D Bioprinting Technique	Application	Reference
Nanocellulose–Alginate	hNC (Human nasoseptal chondrocytes)	Extrusion	Human chondrocytes	(49)
Silk fibroin/gelatin	hTMSCs	Extrusion	Stem cells	(25)
Hyaluronic acid /methylcellulose	MSCs (Mesenchymal stem cells)	Extrusion	Stem cells	(50)
K-carrageenan and gelatin	C2C12 (Mouse myoblasts)	Extrusion	Tissue engineering	(51)
Alginate/cellulose nanocrystal	NIH/3T3 Fibroblast and human hepatoma cells	Extrusion	Tissue engineering	(52)
Silk/gelatin	TVA-BMSCs	Extrusion	Articular cartilage	(53)
Polylactic acid (PLA) /alginate	hASC (human stem cells)	Extrusion	Stem Cells	(54)

2.3 Polymer blends

Polymer blending is a potential fabrication method used for improving the properties of polymers. The desired property of the polymeric system can be obtained by incorporating the correct polymers at appropriate concentrations into the blend. The polymer blends can be categorized into two general classes: immiscible blends and miscible blends. The immiscible blends tend to phase separate; on the contrary, the miscible blends behave homogenous as shown in Figure 2. A crucial factor in determining the performance of the polymer blends is the manipulation of the phase behavior The knowledge of the physicochemical properties controlling the homogeneity of the polymer blend is important to obtain the blends with beneficial characteristics.

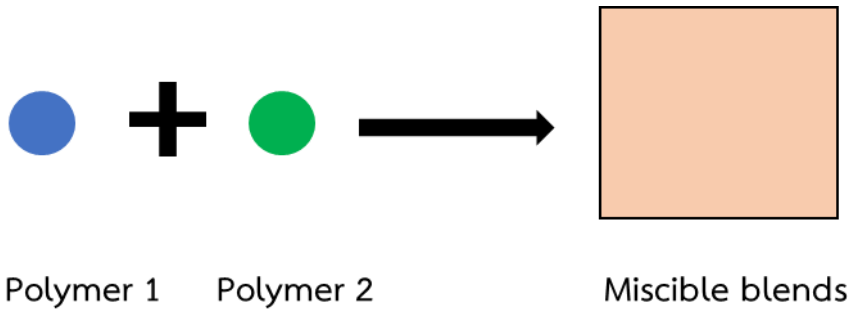

Figure 2. Hypothetical scheme depicting preparation of polymer (55)

2.4 Temperature-Responsive Polymers

Temperature-responsive polymers are “smart” materials that have the ability to response to the change in an environment, such as temperature, pH, ionic strength, light and magnetic field (56). The thermal transition of the temperature-responsive polymers is caused by a change in the polymer-water interaction and/or polymer-polymer interaction. Temperature-responsive polymers are widely used for biomedical applications such as drug delivery, tissue engineering and gene delivery. Temperature-responsive polymers exhibit a phase transition at a certain temperature, causing an abrupt change in the solvent state. There are two types of temperature-

responsive polymers: UCST and lower LCST polymers. LCST is a critical temperature which the LCST polymer and the solvent are completely miscible below. In contrast, the UCST polymer and the solvent are completely miscible at the temperature above UCST. These phase behaviors are shown in Figure 3. The LCST polymer become insoluble upon heating, while the UCST polymer become soluble upon heating (57).

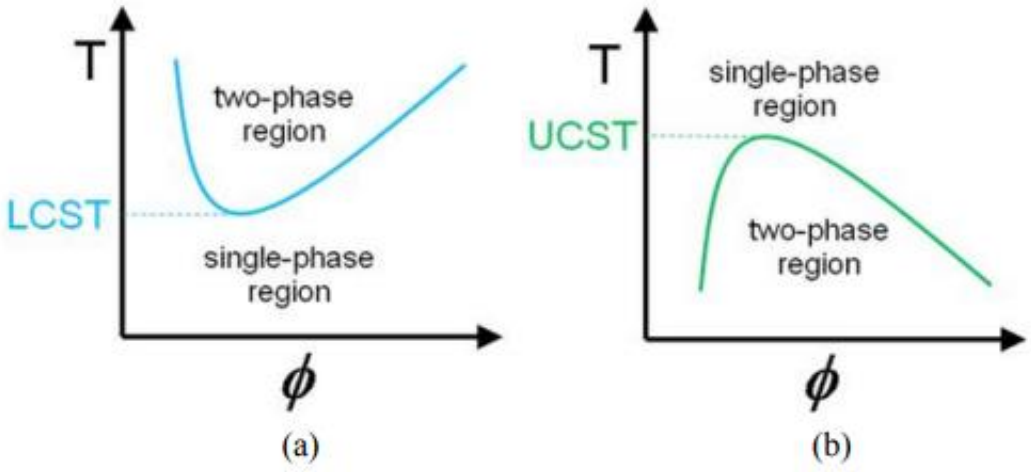

Figure 3. Temperature (T) vs. polymer volume fraction (Ø) (a) LCST polymer and (b) UCST polymer (41)

The temperature-responsive hydrogels are also classified into negative thermo-responsive hydrogels and positive thermo-responsive hydrogels. The negative temperature-responsive hydrogels have the LCST. The interaction between the polymer and the solvent decreases upon heating, causing the gel formation at the temperature above the LCST. In contrast, the positive temperature-sensitive hydrogels have the UCST. The polymer-polymer interaction decreases at temperatures lower than the UCST, leading to gelation at the temperature below UCST (58).

2.5 K-carrageenan (KC)

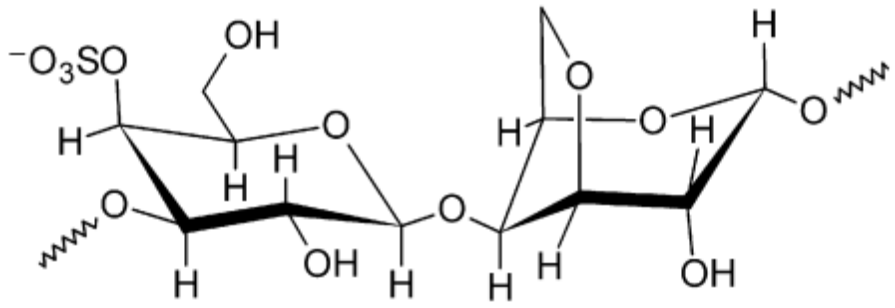

Figure 4. Structural representation of K-carrageenan (59)

K-carrageenan (KC) is a sulphated polysaccharide extracted from red seaweed. The primary structure based on an alternating disaccharide repeating unit of α-(1-3)-d-galactose-4-sulphate and β-(1-4) 3,6-anydro-D-galactose,(60) as shown in Figure 4. KC is widely used in pharmaceutical and food industry for their gelling, thickening, and stabilizing properties. KC forms a thermo-reversible gel depending on its concentration, temperature and the presence of cations such as Ca^{2+}, K^{+} and Na^{+}. The gelation of KC is enhanced primarily by potassium ions, giving firm but brittle gels. Gelation temperature of KC increases as salt concentration increases due to the interaction between salts and negative charged sulphate groups in the KC molecules (61). At high temperature (e.g. above 60 °C), KC can be easily dissolved in water and exists as a random coil structure. During cooling, KC forms a brittle gel and turns to a double helix coil followed by the aggregation of helices, as shown in Figure 5. Nevertheless, KC has other particularly interesting attributes. In addition to its mucoadhesive characteristics, partly due to its molecular interaction with the mucosal tissues (62). KC exhibits inherent thixotropic behavior (60). Therefore, it is interesting to improve the properties of KC-based hydrogel as bioink by combining with other polymers.

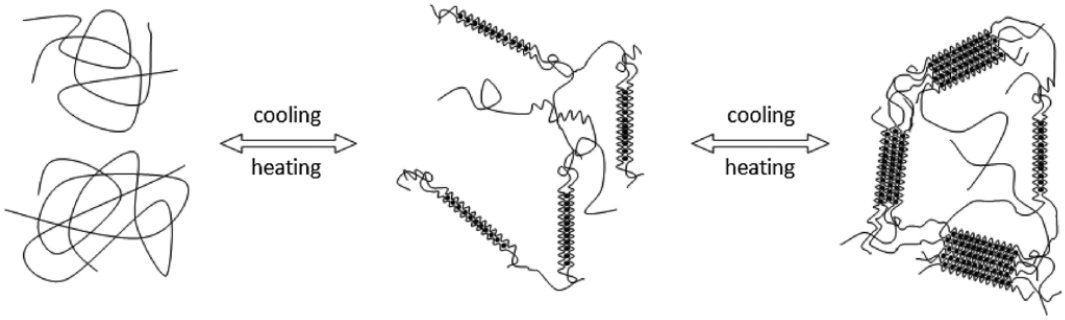

Figure 5. Schematic representation of the thermal reversible gelation mechanism of K-carrageenan (63)

2.6 Methylcellulose (MC)

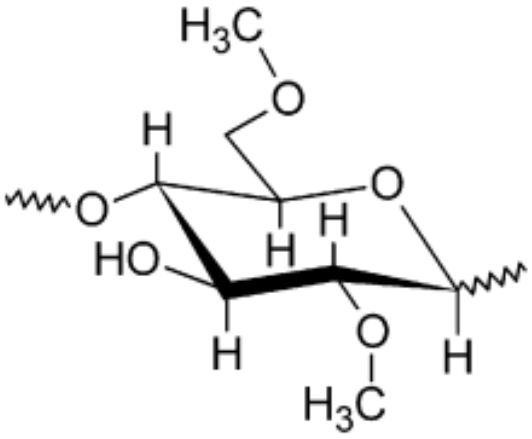

Figure 6. Structural representation methylcellulose building blocks (59)

Methylcellulose (MC) is a water- soluble cellulose polysaccharide derivative. Its synthesized by partial substitution of hydroxyl groups (-OH) with methoxy groups (CH_3O), as shown in Figure 6.(64) MC is widely used as a thickener or binder in cosmetic, pharmaceutical and food applications. MC can form thermoreversible hydrogel upon heating and dissolve upon cooling to low temperature in water (65). However, MC-based hydrogels undergo a sol-gel transition at the lower critical solution temperature (LCST). At low temperature (T < LCST), MC can dissolve in water to become sol (e.g. 30-50 °C for 1% w/w medium viscosity MC). When the temperature is higher than LCST (T > LCST) (e.g., above 50 °C), hydrogen bonds are broken and the

occurring hydrophobic junctions produce gel (Figure 7(a)). The sol-gel transition of MC is varied depending on molecular weight and concentration of MC, degree of methoxy substitution, and additives. In addition, the LCST can be altered by adding ionic compounds to the MC aqueous solution. Salt-in and salt-out ions in the MC solution increase and decrease the LCST, respectively (66). Some salt additives such as NaCl and KCl can lower the gelation temperature of MC solution by increasing the salting out effect in the solution (67). Gelation temperature of MC decreases as salt concentration increases because water molecules tend to surround salt molecules. (Figure 7(b)) (15). The blends of KC which have intrinsic thixotropic behavior and MC which can modify viscosity of the hydrogel may be able to produce a suitable bioink for bioprinting. Furthermore, MC exhibits biocompatibility, non- toxicity and good thixotropic property (68). 3D printing of MC-based hydrogel showed poor mechanical properties. The use of additional materials may be able to improve the mechanical properties of MC

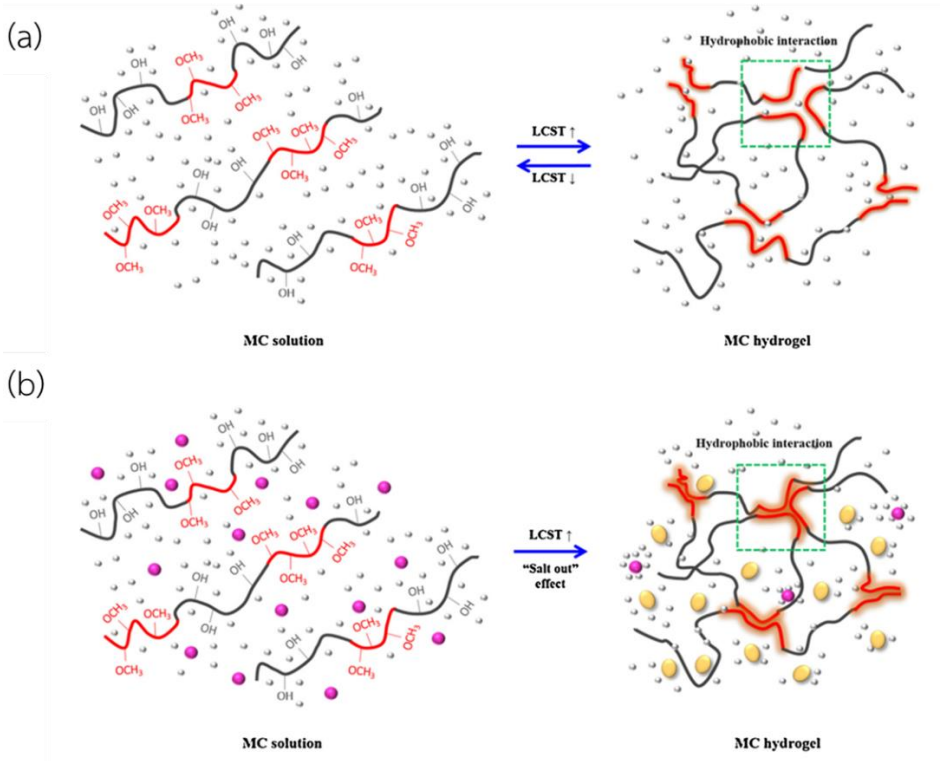

Figure 7. (a) Schematic illustration on the gelation process of pure MC solution and (b) MC solution with salt (66)

2.7 Cellulose nanocrystal (CNC)

Cellulose nanocrystal (CNC) is nanomaterials derived from natural polymer. CNC are strong, light-weight, biodegradable, biocompatible, and renewable natural polymer (69). CNC has attracted great attention due to its excellent biocompatibility, biodegradability, cellular recognition, non- toxicity, and excellent physical and chemical properties (70). CNC has broad application prospects such as in reinforcing fillers and biomedical materials. CNC can be blended into various polymer matrices to increase the mechanical strength and provide substantial shear-thinning property of the bioink.

2.8 Pluronic F127 (PF)

(a)

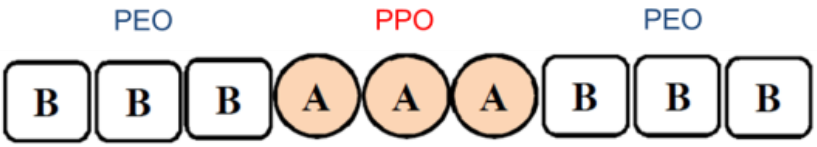

(b)

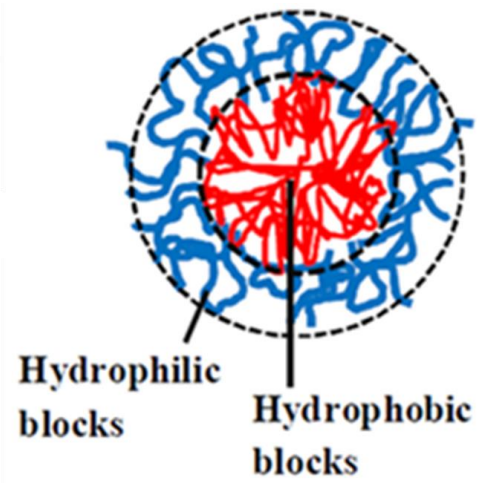

Figure 8. The diagram of (a) the structure of PF and (b) the micelle structure of PF in water (71)

Pluronic F127 (PF) is an amphiphilic block copolymer consisting of hydrophilic PEO and hydrophobic PPO blocks as shown in Figure 8(a). PF in aqueous solution can form self-assembly into micelle at the temperature above critical micelle concentration (CMT). The micelle of PF consists of a hydrophobic core surrounded by a corona of hydrophilic blocks as represented in Figure 8(b).(71)

At low temperature, the aqueous solution of PF remains as liquid. With increasing the temperature, PPO residues become less soluble, and the micellization becomes predominant (72). When the temperature is higher than Critical micelle temperature (CMT), unimers transform into micelles composed of PPO core and PEO corona. The micellization is due to the dehydration of hydrophobic PPO blocks and the subsequent aggregation of the polymer. The temperature is higher than LCST at which the intermicellar interaction occur and the liquid becomes a gel (72). The ordered packing of the micelles causes the gelation of PF as represented in Figure 9.

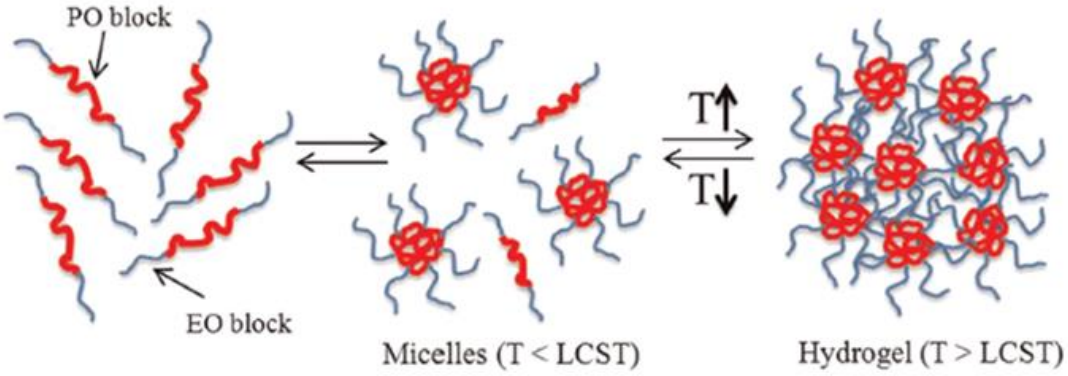

Figure 9. Schematic representation of the gelation mechanism of PF in water (72)

The gel strength of PF depends on temperature and polymer concentration. The strength of the gel increases with the temperature. The gel of PF arises when the concentration of polymer is higher than 15% (73, 74). An increase of the gel strength is the consequence of increasing polymer concentration in water. Besides the concentration of the polymer, the addition of several additives can alter the gel strength. Adding some inorganic salts, such as sodium chloride and sodium monohydrogen phosphate, strengthens the pluronic gel. On the other hand, mixing PF

with some organic molecules such as diclofenac, propylene glycol and ethanol weakens the gel strength (75, 76). The sol-gel transition temperature ($T_{sol-gel}$) is the temperature at which the pluronic liquid turns into gel. The $T_{sol-gel}$ of the PF gel decreases when the polymer concentration increases as shown in Figure 10. In addition, the $T_{sol-gel}$ is affected by the addition of some excipients in the PF gel. The presence of diclofenac, ethanol, propylene glycol or hydrochloric acid increases the $T_{sol-gel}$ of PF while the addition of sodium chloride, sodium hydrogen phosphate, or monosodium phosphate decrease the $T_{sol-gel}$. Although the mechanism of the $T_{sol-gel}$ alteration is not well understood, the change of the dehydration of the hydrophobic blocks of PF may be the key factor. In addition to the $T_{sol-gel}$, some additives also affect the adhesive property of PF. Pluronic itself possesses poor mucoadhesive behavior, but the mucoadhesion of the PF formulation can be enhanced by incorporating another component, ether polymer or small molecule, into the formulation.(77)

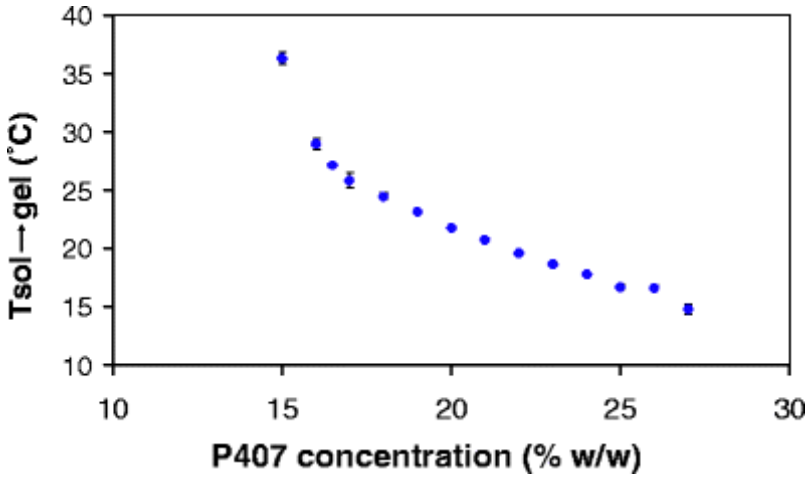

Figure 10. The sol-gel transition temperature versus PF concentration (78)

CHAPTER 3

MATERIALS AND METHODS

3.1 Materials

3.1.1 Chemicals

Methocel® A15 LV 27.5-31.5% methoxy basis was purchased from Sigma-Aldrich (St. Louis,MO). Carageenan, commerial grade, Type I, was purchased from Sigma-Aldrich (St. Louis,MO). Cellulose Nano Crystals/ Cellulose Nano Crystalline (NCCTM) was purchased from CelluForce (Canada Fabriqué au Canada CelluForce NCC®). Pluronic® F-127 was purchased from Sigma-Aldrich (St. Louis,MO). Propidium iodide (Sigma-Aldrich) was purchased from Sigma-Aldrich (Saint Louis, MO). Calcein-AM(Sigma-Aldrich) BioReagent, suitable for fluorescence, ≥96.0% (HPLC) was purchased from Sigma-Aldrich (St. Louis,MO). Dulbecco's phosphate buffered saline (Sigma-Aldrich) modified, without calcium chloride and magnesium chloride, powder, suitable for cell culture was purchased from Sigma-Aldrich (Saint Louis, MO). Dimethyl sulfoxide was purchased from Sigma-Aldrich (St. Louis,MO). Eagle's minimum essential medium (EMEM) was purchased from Sigma-Aldrich (St. Louis,MO). Penicillin streptomycin solution was purchased from Gibco (Grand Island, NY). Trypsin EDTA solution was purchased from Gibco (Grand Island, NY). Horse serum and trypan blue stain (0.4%) were purchased from Gibco by life technologies. Thiazolyl blue tetra-zolium bromide, ≥97.5% (MTT) was purchased from Sigma-Aldrich (St. Louis,MO). Potassium chloride were purchased from Ajax Finechem (Albany, Auckland N.Z.). Phosphate buffered saline powder, pH 7.4, for preparing 1 L solutions was purchased from Sigma-Aldrich (Saint Louis, MO).

3.1.2 Cell line

- Mouse fibroblast L929 cells were purchased from ATCC® CCL-1™ (Manassas, VA)

3.1.3 Instruments

- BIO X 3D bioprinter (CELLINK®, Gothenbure, Sweden)
- Field emission scanning electron microscope (Applied Research Laboratories (SEM-Apreo) FEI Apreo))
- Confocal laser scanning microscope (Model : Zeiss (LMS 800))
- Tensile testing machine (Z010, Zwick Roell, Germany)
- Inverted microscope Axio Vert A1 and Zen Pro software (Carl Zeiss Microscopy GmbH, Göttingen, Germany)
- Discovery hybrid Rrheometer (TA Instruments HR-2, USA)
- Autoclave (HIRAYAMA-HVE-50, Japan)
- CO_2 incubator (CRUMA CO2/S@fegrow 188)
- Freeze dryer (LYOMAX, LSI, USA)
- Biosafety cabinet (BSC) Class II (Esco, AC2-451 Airstream, Singapor
- Microplate reader (BMG : SECTROstar Nano, Germany)
- Analytical balance 4 digit (Mettro Toledo, Model ME204, Switzerland)
- Water bath (Model EWB-111D Esstell)
- Magnetic stirrer (IKA C-MAG HS 7, Germany)
- Test tube 16×125 mm (PYREX®, Mexico)
- Beaker 100 mL, 500 mL and 1,000 mL (PYREX®, Mexico)
- Syringe 1 mL, 3 mL, 5 mL and 10 mL (Nipro, Thailaind)
- Duran bottle 50 mL, 100 mL and 1,000 mL (Duran, Germany)
- Micropipette (Thermo Science KH39789, Finland)
- Cell culture dish 35×10 mm and 60×15 mm (Nunclon™ Delta Surface, China)

- Flask 25 cm^2 and 75 cm^2 (Nunclon™ Delta Surface, China)
- Centrifuge tubes 15 mL and 50 mL (Corning® centristar, Mexico)
- Microcentrifuge tubes 2 mL (Kirgen®, China)
- Magnetic bar 25×8 mm

3.2 Method

In this study overall process of investigation are summarized in the diagram below.

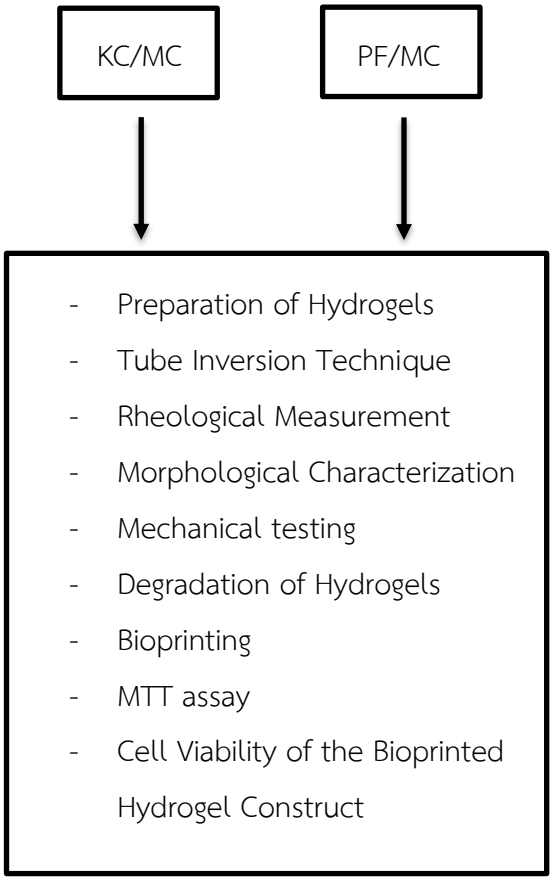

3.2.1 Preparation of Hydrogels

3.2.1.1 K-Carrageenan/Methylcellulose (KC/MC)

KC solution (0.1 to 0.5% w/w) was prepared by dispersing the required quantity of KC in hot water (90 °C) (79). The polymer blends comprising KC (0.1 to 0.5% w/w) and MC (1.0 to 7.0% w/w) were also prepared by mixing the MC solutions with the KC. All solutions are kept in a refrigerator overnight to ensure complete dissolution (63, 80).

3.2.1.2 K-Carrageenan/ Potassium Chloride/ Methylcellulose/ Nanocellulose (KC/KCl/MC/CNC)

The required amount of KCl and CNC was dispersed in the hot solution of KC. Then, the required mass of MC was added into the KC/KCl/CNC mixture before the final weight of the sample was adjusted by adding water. All samples were kept in the refrigerator before use.

3.2.1.3 Pluronic F127/Methylcellulose (PF/MC)

MC solutions (4.0% w/w) were prepared. In brief, the required weight of MC was dispersed in hot water (70 °C) with vigorous stirring and then the remaining hot water was added into the dispersion to produce the sample with a final weight of 100 g. The solutions were kept in a refrigerator overnight to ensure complete dissolution (80). PF (16 to 22% w/w) were blended with MC using a cold method as previously described (81). The required weight of PF powder was dispersed in the cold solution of MC. After PF powder was thoroughly wetted, the cold water was added to obtain the PF/MC blends with a final weight of 100 g. The blends were then transferred to a refrigerator and kept overnight prior to use.

3.2.1.4 Preparation of cell-suspended bioink for the cell viability studies

The mixture of KC/KCl/CNC was sterilized using an autoclave for 30 min at 120 °C (12) MC powder sterilized using ethylene oxide gas as previously described (82) was dispersed into these solutions to obtain 0.3KC/ 7MC/ 0.1KCl/ 2CNC and 0.3KC/7MC/0.1KCl/4CNC. PF powder sterilized with UV light (UV-C at 253.7 nm) for 1 h (83). The mixture of PF and MC, PF and MC powders were sterilized before use and sterilized water was employed in the sample preparation processes as previously described (26). In brief, MC sterilized powders were dispersed in water and PF sterilized powders was dispersed into these MC solutions to obtain 18PF/4MC and 20PF/4MC.

3.2.2 Test tube tilting method (TTM) analysis

The gelation temperature of samples was observed using the test tube inversion method. One mL of the sample was added into a test tube. The test tube containing the sample was placed in a water bath. The samples were equilibrated for 5 min at each temperature. The temperature of the water bath was increased in 1 °C increments. The temperature at which the sample did not flow upon tube inversion was considered as the gelation temperature. The sample with gelation temperature in the range of 30 °C to 37 °C was selected for further analysis (84). Sol-gel transition was evaluated by tilting the tube after the incubation phase. The temperature at which the samples became solid but slightly flowed at the surface when tilting the tube was recorded as gelation temperature of a soft gel. When heating, the temperature at which samples did not flow was recorded as a transition temperature of a hard or strong gel (85).

3.2.3 Rheological Measurement

The determination of rheological behaviors of hydrogels is necessary to test their shear-thinning and thixotropic properties. All rheological characteristics of hydrogels were measured using a plate rheometer (Discovery Hybrid Rheometer, DHR; TA Instruments, USA, Figure 11) equipped with a cone plate geometry (diameter 60 mm cone angle 2°). For steady flow test, the viscosity curves were recorded with increasing shear rate at a constant temperature of 25 ℃. All tests were carried out in triplicate.

The analysis of the thixotropic properties/recoverability of the hydrogels was performed as described by Li et al. (51) The rheological properties of hydrogels before (step I), during (step II), and after (step III) the printing process were simulated. At step I, a shear rate of 0.1 s^{-1} was applied for 60 s, which simulates the initial state of a hydrogel before printing. Step II simulates the sheared hydrogel during extrusion. The shear rate of 100 s^{-1} was applied and held for 5 s before moving to step III (51). At step III, the shear rate was reduced to 0.1 s^{-1} again and held for 60 s. This step simulates the final state of the hydrogel after printing.

Figure 11. Discovery Hybrid Rheometer, DHR; TA Instruments, USA (From: https://osit.psu.ac.th/th/equipment/)

3.2.4 Morphological Characterization

The morphology of the hydrogels was evaluated using scanning electron microscopy (Field Emission Scanning Electron Microscope Applied Research Laboratories (SEM-Apreo) FEI Apreo, Figure 12). The hydrogel samples are frozen in a freezer at -30℃ for 24h, and then freeze dried for 1 days. The top and cross-sectional surfaces are imaged under SEM, whereby the cross-sectional structures are obtained by fracturing the samples in liquid nitrogen (86).

Figure 12. SEM-Apreo FEI Apreo (From: https://osit.psu.ac.th/th/equipment/)

3.2.5 Mechanical property measurements

The mechanical measurements of hydrogels were tested by a uniaxial compression tester (Tensile Testing Machine, Z010, Zwick Roell, Germany, Figure 13) with a 100N load cell at room temperature. The samples with cylindrical shape (20 mm in diameter and 10 mm in height) were prepared. The tests were performed at a compression speed of 0.5 mm s^{-1} at 30% strains. Each bioink formulation was measured at least in triplicate (86).

Figure 13. Tensile Testing Machine, Z010, Zwick Roell, Germany (From: https://osit.psu.ac.th/th/equipment/)

3.2.6 Degradation of Hydrogels

The in vitro degradation of the hydrogel was observed by gravimetric method as previously described. The cast cylindrical sample (15 mm in diameter and 8 mm in height) were examined for 30 days in deionized water at 37 °C as previously described (86). At definite time intervals, the samples were dabbed dry and weighed. The relative percentage of degradation (W_r) is calculated by

$$W_r = (W_1/W_0) \times 100\%,$$

where W_0 and W_1 are the weights of a hydrogel sample before and after soaking, respectively.

3.2.7 Preparation of cell-suspended bioink

Mouse fibroblast cells L929 were used due to their extensive role in toxicity detection. L929 cells are cultured and expanded before bioprinting. The cells are cultured in the cell culture media of Eagle's Minimum essential medium (EMEM) supplemented with 10% fetal bovine serum and 1% antibiotics (100 µ/mL of penicillin G and 100 mg/mL of streptomycin). To increase the cell numbers, cells are replaced

with fresh medium every 2 days. The culture medium was completely aspirated, then 3 mL sterile PBS was added of the plate, gently swirled, then completely aspirated. 1 mL of sterile trypsin + EDTA was added, and the plate was gently swirled so the mixture coated the entire surface of the plate. The trypsin + EDTA was aspirated, and the plate was incubated for 5 min at 37 ℃ and 5% CO2. Then 10 mL of DMEM were added into flask (13). The cultures are kept in an incubator (5% CO_2 and 95% air) at 37 ℃. The appropriate concentrations of hydrogels and cells were mixed at a volume ratio of 9:1 using cellmixer (CELLINK®, Gothenburg, Sweden), resulting in a final concentration of 3×10^5 cells mL^{-1} in 0.3KC/7MC/0.1KCl/2CNC and 0.3KC/7MC/0.1KCl/4CNC.

3.2.8 Bioprinting

Cell free and cell-laden hydrogels were bioprinted layer-by-layer using the BIO X 3D Bioprinter (CELLINK®, Gothenbure. Sweden, Figure 14). A 3D bioprinter was used to print hydrogel composite structures and the 3-D structures of the scaffolds are designed using the printer software. A grid pattern (10 mm long, 10 wide and 0.3 thick) for printability experiment was designed with CAD software and exported as stereolithography (stl) files. The cell suspension was added to the hydrogel, resulting in a final cell concentration of 3×10^5 cells/mL in the hydrogel. (51, 87) Cell-hydrogel mixtures were placed into extrusion cartridges which were placed on the printing carriage of 3D printer for extrusion through a 27-gauge needles. Each hydrogel was loaded into a syringe at 25 ℃ for use with the 3D bioprinter and a heat plate at 37 ℃ was positioned below the print head. An extrusion-based printing process is selected for printing the material onto a Petri dish under the suitable condition. The 3D structure is constructed in a layer-by-layer manner. The bioprinted constructs were cultured in the incubator of 37 ℃ for up to 5 days (15). The bioprinted construct was observed under a microscope (Zeiss Axio Vert Al and Zen Pro Software, Carl Zeiss Microscopy GmbH, Göttingen, Germany, Figure 15.) Three samples of each hydrogel were used for each printability test.

Figure 14. CELLINK®, Gothenbure. Sweden (From: https://www.cellink.com/cellink-featured-3d-bioprinting-article-south-china-morning-post/)

Figure 15. Zeiss Axio Vert Al and Zen Pro Software, Carl Zeiss Microscopy GmbH, Göttingen, Germany (From: https://mikroskop.com.pl/pdf/Broszura-Zeiss-Axio-Imager.pdf)

3.2.9 MTT assay

Cytotoxicity testing was performed using L929 cells according to USP42-NF37 (88). Sample (0.2 g.) from the refrigerator was incubated at 37 °C for 30 min to obtain a required hydrogel. Then, the hydrogel was extracted with 1 mL of culture EMEM for 24 h at 37 °C and the extraction was filter sterilized (89). A cell suspension of 2 $\times 10^5$ cells/ml L929 (100 µl/well) in Eagle's Minimum essential medium (EMEM) was seeded into a 96-well plate and incubated at 37 °C, with 5% CO_2 at 95% air for 24 h. After incubation, the media was removed and rinse with PBS twice (100 mL). The wells are inoculated with 100 mL of the extract solutions of the cell encapsulated hydrogels and incubated in DMEM at 37 °C, 5% CO_2 for 24 h (26). Ethyl alcohol and the cell culture medium, are used as a positive and negative control, respectively (90, 91). Media are removed and washed with 100 mL of PBS twice and the PBS is then removed. The samples were added, then the plates were incubated at 37 °C, 5% CO2 incubator for 24 hours. After 24 hours incubation, the samples were removed and rinse with PBS twice. Then 100 µl/well of 0.5 mg/ml MTT solution was added and the plate was incubated for 4 hours. MTT solution was suck off and formazan crystal was dissolved with 100 µl/well of DMSO. The viability was calculated as the ratio between a blank and the sample absorbance measured using a microplate reader at 570 nm.

3.2.10 Cell Viability of the Bioprinted Hydrogel Construct

Cell viability in the bioprinted constructs was examined immediately after bioprinting using live/dead cell-imaging assay. The bioprinted constructs were washed twice with PBS and incubated for 15 min at 37 °C with DPBS solution containing 5 umol/L propidium iodide and 2 umol/L calcein acetoxymethyl ester for 15 min and rinsed with PBS before investigated via a confocal laser scanning microscope (Zeiss LSM800, Carl Zeiss Microscopy GmbH, Germany, Figure 16). The cell viability, the ratio of the number of live cells to the number of total cells, was evaluated manually from the CLMS readings.

Figure 16. Zeiss LSM800, Carl Zeiss Microscopy GmbH, Germany (From: https://www.photonics.com/Products/Compact_Confocal_Microscope/pr56973)

3.2.11 Statistical analysis

All data were expressed as mean ± standard deviation and compared statistically by means of variance (ANOVA) coupled with Tukey's test. Differences were statistically significant when $p \leq 0.05$.

CHAPTER 4

RESULTS AND DISCUSSION

4.1 KC/MC based hydrogels (92)

4.1.1 Test tube tilting method (TTM) analysis

Based on test tube inversion results in Table 4.1, the mean values of the gelation temperature of 0.1KC/MC, 0.2KC/1MC, 0.3KC/MC, 0.5KC/1MC, 1KC/1MC, 1KC/2MC were gel in refrigerator only (61). Mixtures with higher concentrations of MC such as 0.1KC/5MC and 0.2KC/5MC were in a sol state at 4 °C and room temperature (25 °C) and became soft gel at body temperature (37 °C) and turned to hard gel at 40 °C. In addition, the mixture of 0.2KC/7MC and 0.3KC/7MC was solution at room temperature but turned to gel at 37 °C, but 0.3KC/7MC provided stronger gel than 0.2KC/7MC.

Moreover, salt can be used as ionic cross-linker to modulate the gelation of KC/MC (13). Therefore, various concentrations of salts including KCl was used to strengthen the 0.3KC/7MC blend. Physical cross-linking, a non-chemical abut that utilizes ionic interactions can increase the mechanical property of hydrogels. The blends of low concentrations of salts, 0.3KC/7MC/0.01KCl was sol at room temperature and became weak gel at 37 °C. Furthermore, the blends of 0.3KC/7MC/0.05KCl and 0.3KC/7MC/0.1KCl (higher salt concentrations) were soft gel at room temperature and became slightly stronger gel at 37 °C. However, when increasing concentrations of KCl the mixtures of 0.3KC/7MC/0.2KCl was solution at room temperature and behaved gel at 37 °C. Therefore, only single salt of 0.1KCl was mixed in the 0.3KC/7MC blend in further formulations. 0.3KC/7MC/0.1KCl was mixed with various concentrations of CNC to further enhance the mechanical strength. Based on TTM, the mixtures of 0.3KC/7MC/0.1KCl/0.05CNC, 0.3KC/7MC/0.1KCl/0.1CNC, 0.3KC/7MC/0.1KCl/0.2CNC, 0.3KC/7MC/0.1KCl/0.5CNC, 0.3KC/7MC/0.1KCl/1CNC, 0.3KC/7MC/0.1KCl/2CNC and

0.3KC/7MC/0.1KCl/4CNC provided soft gel at room temperature and strong gel at 37°C. Consequently, the blends of 0.3KC/7MC/0.1KCl and various amounts of CNC were further analysed in the printing experiments.

Table 4.1 The gelation temperature (mean±SD, n=3) of the mixtures of KC and MC determined by the tube inversion method

Formulation	4 °C	25 °C	37 °C
0.1KC/1MC	Gel	Sol	Sol
0.2KC/1MC	Gel	Sol	Sol
0.3KC/1MC	Gel	Sol	Sol
0.5KC/1MC	Gel	Sol	Sol
1KC/1MC	Gel	Sol	Sol
1KC/2MC	Gel	Sol	Sol
0.1KC/5MC	Sol	Sol	Soft gel
0.2KC/5MC	Sol	Sol	Soft gel
0.2KC/7MC	Sol	Sol	Soft gel
0.3KC/7MC	Sol	Sol	Soft gel
0.3KC/7MC/0.01KCl	Sol	Sol	Soft gel
0.3KC/7MC/0.05KCl	Soft gel	Soft gel	Stronger gel
0.3KC/7MC/0.1KCl	Soft gel	Soft gel	Stronger gel
0.3KC/7MC/0.2KCl	Sol	Sol	Sol
0.3KC/7MC/0.1KCl/0.05CNC	Soft gel	Soft gel	Stronger gel
0.3KC/7MC/0.1KCl/0.1CNC	Soft gel	Soft gel	Stronger gel
0.3KC/7MC/0.1KCl/0.2CNC	Soft gel	Soft gel	Stronger gel
0.3KC/7MC/0.1KCl/0.5CNC	Soft gel	Soft gel	Stronger gel
0.3KC/7MC/0.1KCl/1CNC	Soft gel	Soft gel	Stronger gel
0.3KC/7MC/0.1KCl/2CNC	Soft gel	Soft gel	Stronger gel
0.3KC/7MC/0.1KCl/4CNC	Soft gel	Soft gel	Stronger gel

The occurrence of gel or sol of these mixtures depended on the characteristics of each component. Methylcellulose (MC) is a water-soluble cellulose polysaccharide derivative. MC has inverse thermal gelling properties. The chemical structure of MC is characterized by the presence of both hydrophilic hydroxy (–OH) and hydrophobic methoxy groups (–OCH3). At low temperature, MC can dissolve in water to become sol (e.g. 30-50°C for 1% w/w medium viscosity MC). However, at high temperature, hydrogen bonds are broken and the occurring hydrophobic junctions produce gel (e.g. above 50°C) (15). The gelation temperature of MC also depends on its concentration and the added salts. Gelation temperature of MC decreases as salt concentration increases because water molecules tend to surround salt molecules (61).

KCl can reduce the gelation temperature of MC and categorized as a salting out agent. due to the greater hydration ability of chloride ions that can attract more water molecules than MC (93). The association of chloride ions with water decreases the solubility of MC in water, lowers the temperature of hydrophobic aggregation of MC chains and promotes the formation of a gel network structure (67, 94).

KC is a sulphated polysaccharide extracted from red seaweed. KC forms a thermo-reversible gel depending on its concentration, temperature and the presence of cations such as Ca^{2+}, K^{+} and Na^{+}. Gelation temperature of KC increases as salt concentration increases due to the interaction between salts (KCl) and negative charged sulphate groups in the KC molecules (61). At high temperature (e.g. above 60°C), KC can be easily dissolved in water and presents a random coil structure. During cooling, KC forms a brittle gel and presents a double helix coil followed by the aggregation of helices. However, CNC is also rich in hydroxyl (OH) groups in the structure (95). The hydrogen bonds between the hydroxyl groups of CNC and the polymer matrix can be increase mechanical strength and improve the bioink properties (92).

4.1.2 Printability

The printed constructs of 0.3KC/7MC/0.1KCl mixtures including 0.3KC/7MC/0.1KCl/0.05CNC, 0.3KC/7MC/0.1KCl/0.1CNC, 0.3KC/7MC/0.1KCl/0.2CNC, 0.3KC/7MC/0.1KCl/0.5CNC, 0.3KC/7MC/0.1KCl/1CNC were brittle and showed poor shape fidelity. According to Ouyang et al., for one-layered grids, a bioink with a good printability should produce a fabricated structure where the regular grids and square holes conform to the pre-designed pattern (96). On the other hand, a printed grid shows a hydrogel with poor printability formed almost circular holes. From Figure 17(a), 0.3KC/7MC/0.1KCl/4CNC showed excellent regularity with square holes but 0.3KC/7MC/0.1KCl/2CNC formed rather circular-like holes. Figure 17(b) presents the 3D structures of ten layers of both 0.3KC/7MC/0.1KCl/2CNC and 0.3KC/7MC/0.1KCl/4CNC. On the basis of Ouyang's criterion, 0.3KC/7MC/0.1KCl/4CNC with higher concentration of CNC exhibited a much higher printability than 0.3KC/7MC/0.1KCl/2CNC. These results indicated that increasing the concentration of CNC resulted in more printability.

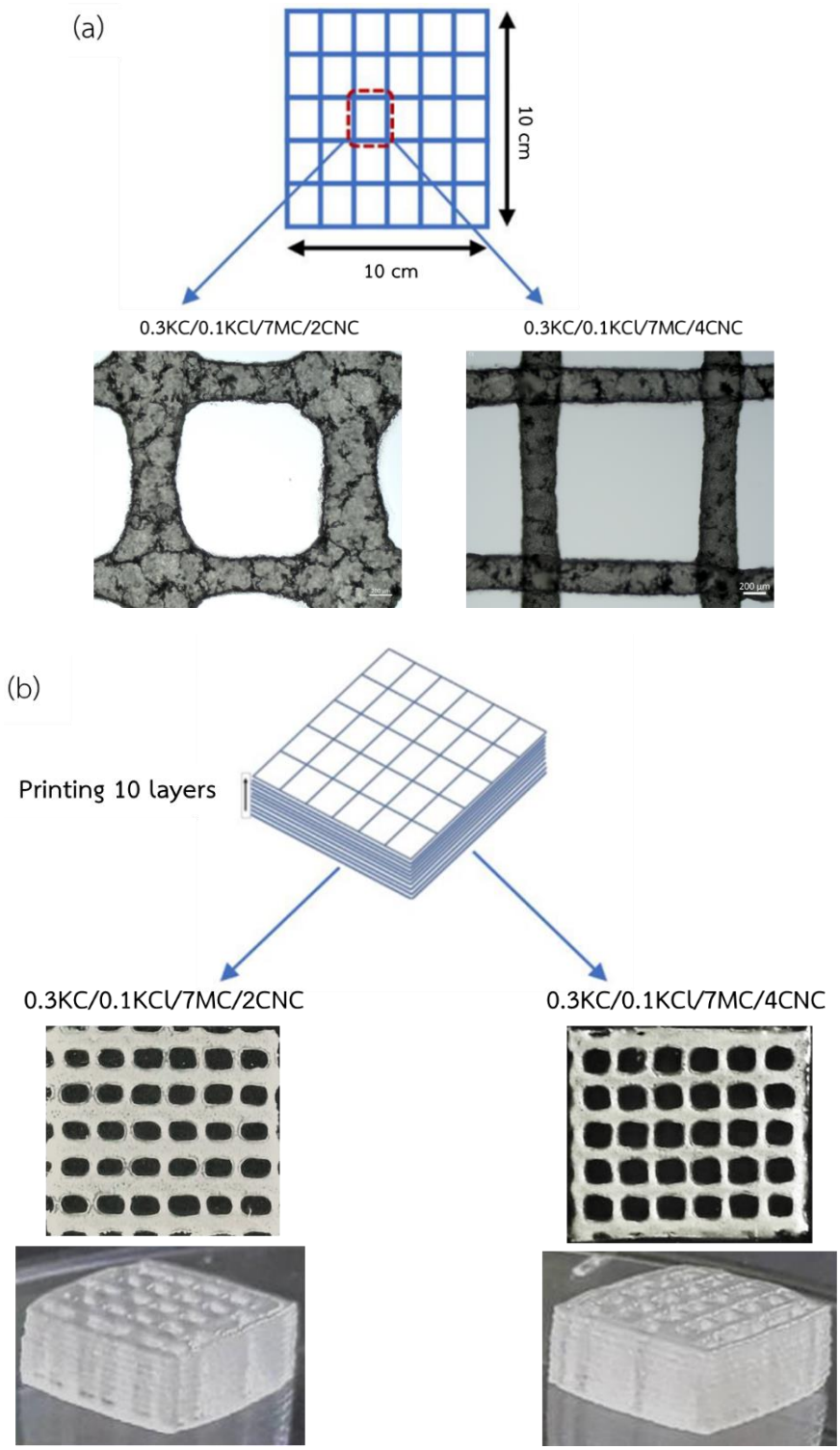

Figure 17. Optical microscopic (OM) images of the first layer of 0.3KC/0.1KCl/7MC/2CNC and 0.3KC/0.1KCl/7MC/4CNC bioprinted grid (scale bar, 200 µm) and (b) 3D-printed 10-layered structure of both 0.3KC/0.1KCl/7MC/2CNC and 0.3KC/0.1KCl/7MC/4CNC hydrogels.

4.1.3 Rheological evaluation

Rheological properties of hydrogels particularly shear-thinning and quick recovery characteristics have a major influence on shape fidelity and hydrogels printability in extrusion printing. The viscosity of both 0.3KC/0.1KCl/7MC/2CNC and 0.3KC/0.1KCl/7MC/4CNC decreased as the shear rate increased as shown in Figure 18. Both 0.3KC/0.1KCl/7MC/2CNC and 0.3KC/0.1KCl/7MC/4CNC yielded a confidence fit of R2 ≥ 0.95, R2 values of the straight fitting lines of 0.3KC/0.1KCl/7MC/2CNC and 0.3KC/0.1KCl/7MC/4CNC were 0.9952 and 0.9855, respectively (97). The obtained n value of 0.3KC/0.1KCl/7MC/2CNC and 0.3KC/0.1KCl/7MC/4CNC were 0.52 and 0.45, respectively. This suggested that both formulations are shear- thinning in nature.

A model that mathematically described shear-thinning fluids was the power law equation (98).

$$\eta = K\dot{\gamma}^{n-1}$$

where η is viscosity, $\dot{\gamma}$ is shear rate, K is the consistency index (K) and n is the flow index. Flow index could be determined from the intercept and the slope of straight line applied from the plot of log η versus log $\dot{\gamma}$. The n value expressed the materials ability to thicken, thin, or remain Newtonian. A flow index (n) approached 1 for Newtonian fluid, while this index of less than one suggested shear- thinning material (97, 99, 100). When the n value decreased with increasing CNC concentration. The decreasing n value indicated the stronger shear- thinning behavior (99, 101, 102). A previous study reported that the shear-thinning property of a bioink could be improved by the incorporation with the nanocellulose materials (103). The decrease in the n value could be explained by an increase in entanglements with increasing CNC (100).

The thixotropic systems showed a characteristic time of viscosity recovery behavior (103, 104). In this study, the thixotropic property of the 0.3KC/0.1KCl/7MC/2CNC and 0.3KC/0.1KCl/7MC/4CNC samples was determined to simulate the rheological behaviors of hydrogels before (step I), during (step II), and after (step III) the 3D printing process. The recovery behavior was determined through three steps: low-high-low (step I- step II-step III) shear rate as shown in Figure 19. Both hydrogels present a thixotropic property. The viscosity of 0.3KC/0.1KCl/7MC/2CNC and

0.3KC/0.1KCl/7MC/4CNC recovered to 82.43% and 60.13% of the initial viscosity, respectively, in about 30 s after the high shear rate was removed. Although, based on printability experiment, 0.3KC/0.1KCl/7MC/4CNC showed better printability than 0.3KC/0.1KCl/7MC/2CNC. It was found that for a highly viscous hydrogel to have a good printability for the extrusion-based printing, the hydrogel is required to have a shear thinning property during printing and should be highly thixotropic after printing (8). The viscosity of a hydrogel recovered after a period of rest because the broken cross-links caused by shearing need time to be rebuilt (86). 0.3KC/0.1Kl/7MC/4CNC has a high viscosity at low shear rates and is shear thinning. The high viscosity gives excellent shape fidelity when printed.

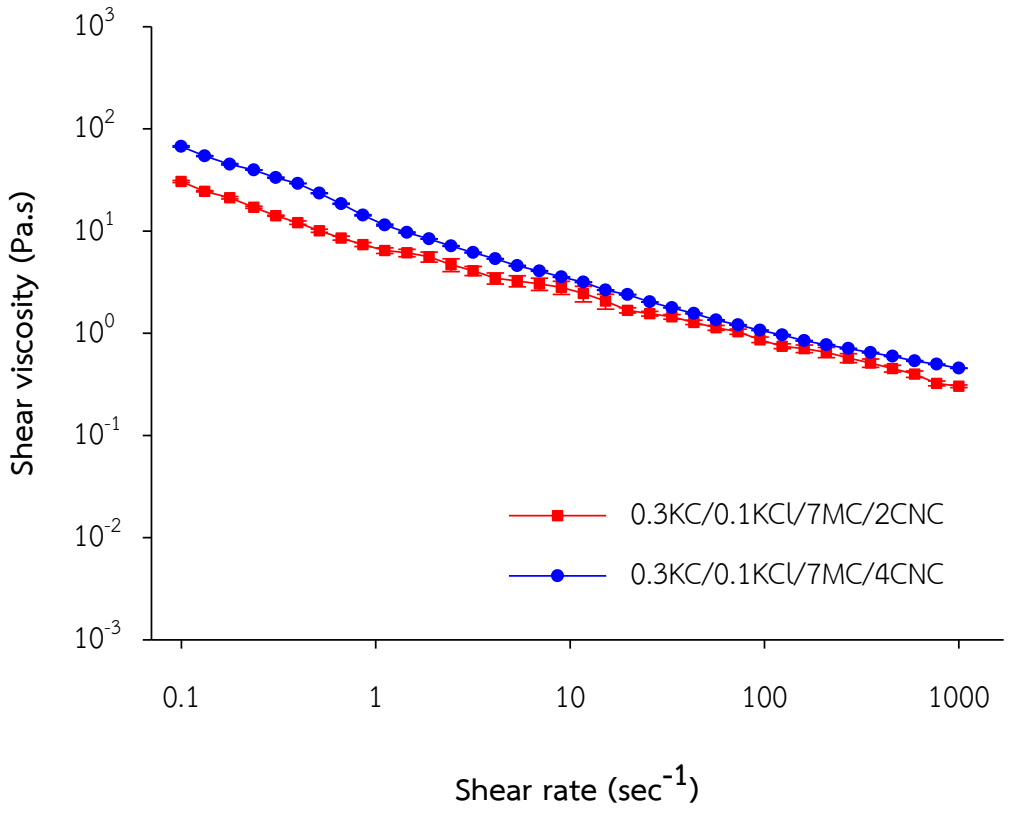

Figure 18. Rheological properties for 0.3KC/0.1KCl/7MC/2CNC and 0.3KC/0.1KCl/7MC/4CNC hydrogels at 25 °C: viscosity as a function of shear rate

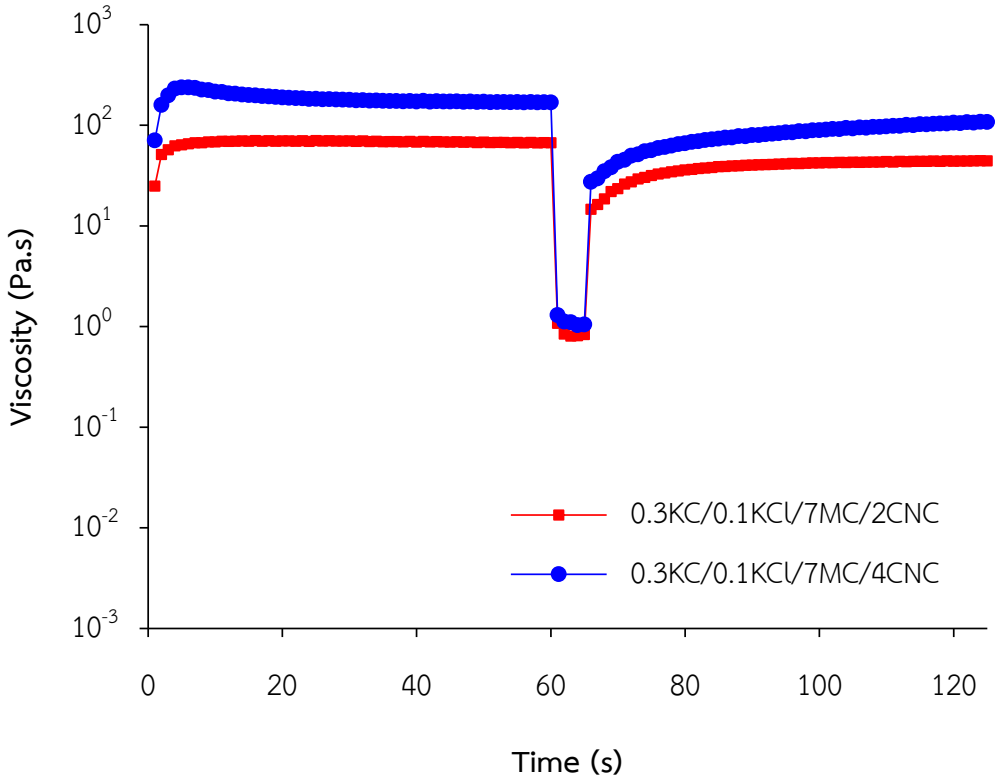

Figure 19. Recovery behavior of the hydrogels, the printing process simulated by the rheological study: step I, before printing; step II, during printing; and step III, after printing.

4.1.4 Morphological characterizations

The morphology of hydrogel was examined using FE-SEM. It was used to create the detailed pore structure of 0.3KC/0.1KCl/7MC, 0.3KC/0.1KCl/7MC/2CNC and 0.3KC/0.1KCl/7MC/4CNC hydrogels and to consider the effect of CNC on the microstructure of the hydrogel. The microstructure of 0.3KC/0.1KCl/7MC, 0.3KC/0.1KCl/7MC/2CNC and 0.3KC/0.1KCl/7MC/4CNC hydrogels were observed as shown in Figure 20. The 0.3KC/0.1KCl/7MC hydrogel has a smooth surface with smaller pore sizes than the 0.3KC/0.1KCl/7MC/2CNC and 0.3KC/0.1KCl/7MC/4CNC hydrogels, Figure 20. (a-b). The incorporation of CNC in the mixtures of 0.3KC/0.1KCl/7MC resulted in a lower porous microstructure. The pore size of 0.3KC/0.1KCl/7MC/2CNC was about 70 – 80 μm (Figure 20. (c-d)). With higher content of CNC, the pore size of

0.3KC/0.1KCl/7MC/4CNC decreased considerably to about 10 - 30 μm, Fig. 3(e-f). The smooth surface of the pore walls of the hydrogel containing CNC indicates the absence of CNC aggregation and homogenous dispersion of CNC in the 0.3KC/0.1KCl/7MC hydrogel (52).

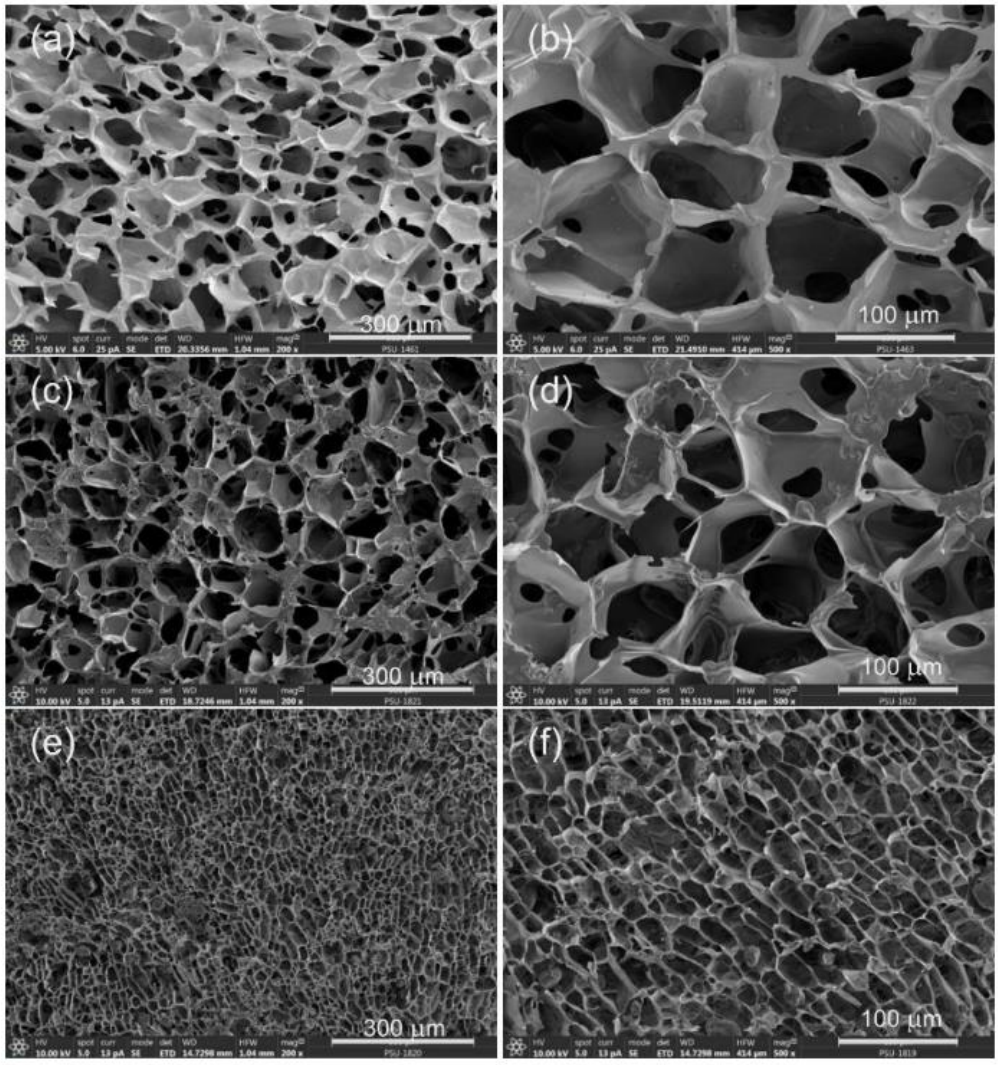

Figure 20. Scanning electron micrographs of freeze-dried (a-b) 0.3KC/0.1KCl/7MC, (c-d) 0.3KC/0.1KCl/7MC/2CNC and (e-f) 0.3KC/0.1KCl/7MC hydrogels.

4.1.5 Compression test

The mechanical properties of the prepared hydrogels were characterized by compression test at surrounding temperature. The strain-stress curves for 0.3KC/0.1KCl/7MC/2CNC and 0.3KC/0.1KCl/7MC/4CNC samples are shown in Figure 21. The compressive stress of 0. 3KC/ 0. 1KCl/ 7MC, 0. 3KC/ 0. 1KCl/ 7MC/ 2CNC and 0.3KC/0.1KCl/7MC/4CNC hydrogels was computed to be 6.43 ± 0.41, 20.03 ± 0.02 and 23.28 ± 0.01 kPa, respectively (Figure 22.). Without the addition of CNC, the 0.3KC/0.1KCl/7MC hydrogel showed the lowest value. By adding CNC, the above compressive stress was obtained. Moreover, 0.3KC/0.1KCl/7MC/2CNC sample showed significantly lower compressive stress than 0.3KC/0.1KCl/7MC/4CNC ($p < 0.001$). This suggested that the compressive stress increased with increasing CNC content, and CNC was advantage for improving the mechanical strength of the samples.

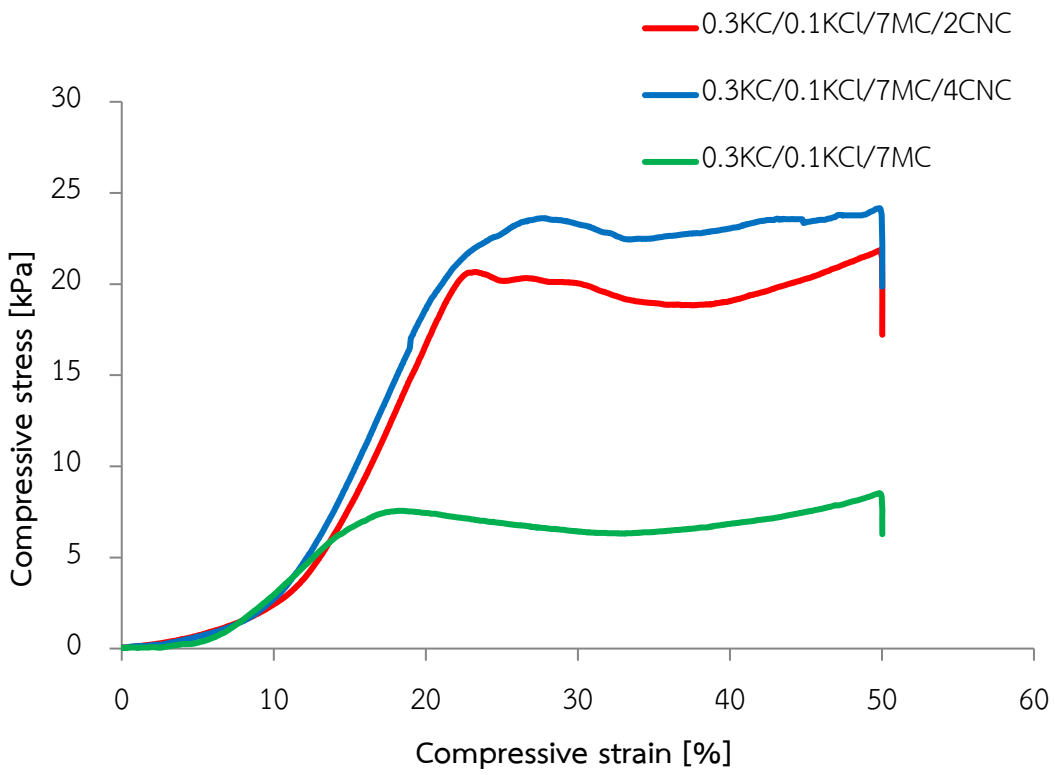

Figure 21. Compressive stress-strain curves for 0.3KC/0.1KCl/7MC, 0.3KC/0.1KCl/7MC/2CNC and 0.3KC/0.1KCl/7MC/4CNC hydrogels.

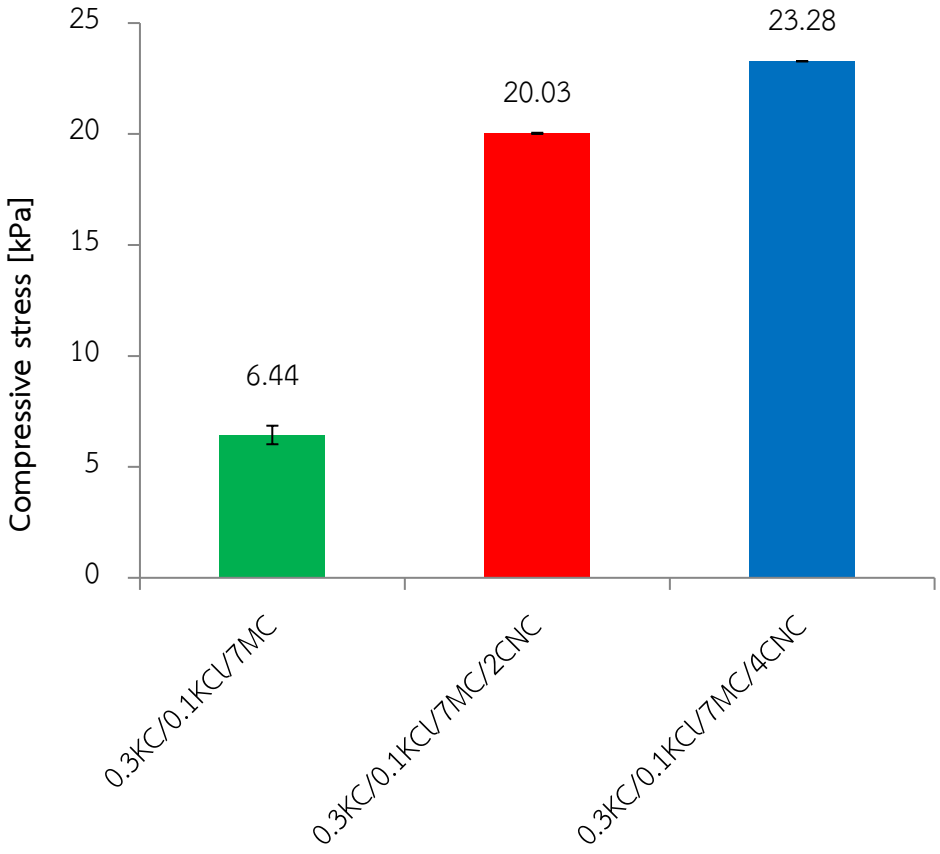

Figure 22. Compressive stress of 0.3KC/0.1KCl/7MC, 0.3KC/0.1KCl/7MC/2CNC and 0.3KC/0.1KCl/7MC/4CNC hydrogels.

4.1.6 Degradation of 0.3KC/7MC/0.1KCl/2CNC and 0.3KC/0.1KCl/7MC/4CNC hydrogels

The degradation of the hydrogels over time is presented in Figure 23. The weight loss of 0.3KC/7MC/0.1KCl/2CNC hydrogel at day 1, 4, 7, 14,21 and 30 was 100.23 ± 0.20, 81.82 ± 0.77, 71.12 ± 0.29, 40.63 ± 0.74, 30.39 ± 0.32 and 10.88 ± 0.83 %, respectively. Those of 0.3KC/0.1KCl/7MC/4CNC hydrogel at day 1, 4, 7, 14, 21 and 30 was 100.35 ± 0.28, 83.01 ± 0.70, 74.35 ± 0.53, 46.09 ± 0.82, 31.82 ± 0.85 and 13.36 ± 0.63 %, respectively. Degradation of hydrogel with higher content of CNC (0.3KC/0.1KCl/7MC/4CNC), was slightly lower than that with lower CNC content, i.e.,

0.3KC/7MC/0.1KCl/2CNC. Therefore, the addition of CNC to the hydrogels affected their degradation. Previous research had also shown that physical blending can decrease the degradation of hydrogels by promote hydrogen bond interaction between gel elements. (105, 106). The hydrogen bonds between CNC and the polymers (KC and/or MC) may retard the extent of gel degradation. These analysis suggest that CNC may be used to modulate hydrogel degradation.

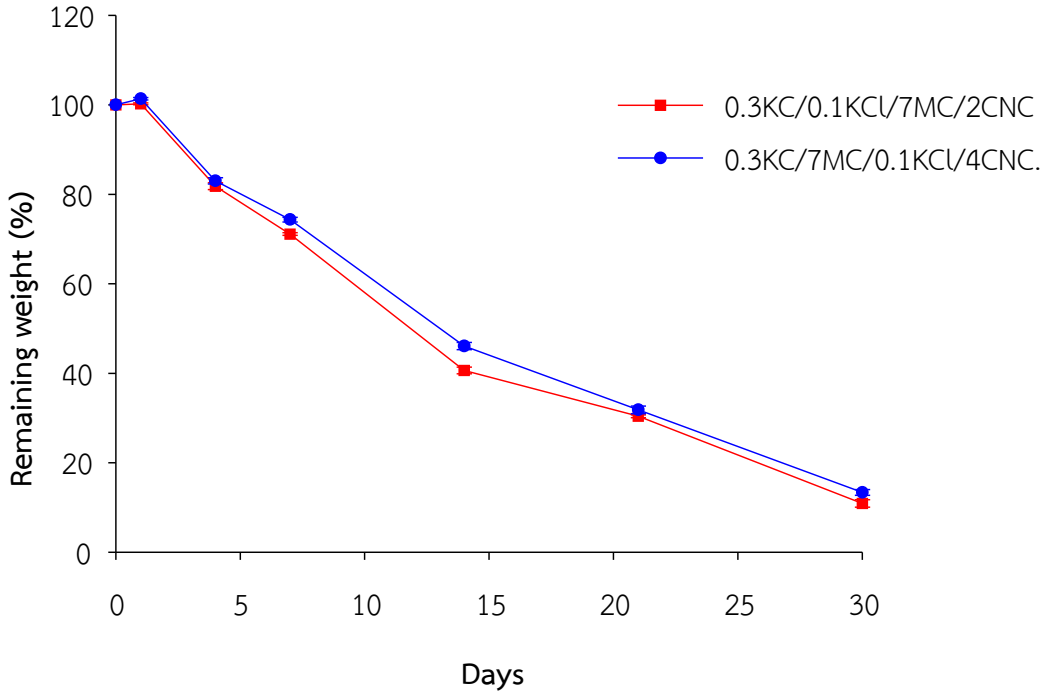

Figure 23. In vitro degradation of 0.3KC/0.1KCl/7MC/2CNC and0.3KC/0.1KCl/7MC/4CNC hydrogels in deionized water at 37 °C.

4.1.7 Cytotoxicity analysis

Cytotoxicity test was performed to evaluate any potential toxic effects of the hydrogels on cell viability. The result of cytotoxicity assay is shown in Figure 24. Cell viability of the negative control (cell culture medium), positive control (ethanol), 0.3KC/0.1KCl/7MC, 0.3KC/0.1KCl/7MC/2CNC and 0.3KC/0.1KCl/7MC /4CNC was 100.0 ± 0.89%, 8.67 ± 0.99%, 94.57 ± 1.48%, 92.12 ± 2.30 and 90.34 ± 2.05%,

respectively. Cell viability of hydrogels was significantly different from each other ($p < 0.05$) and lower than that of negative control ($p < 0.01$). Furthermore, cell viability was lower in the presence of CNC. However, the value of cell viability above 70% was considered without cytotoxic potential (49). Therefore, the evaluated hydrogels may not cause any potential toxic effects on the tested cell lines and have good potential as biomaterials for tissue engineering and 3D bioprinting.

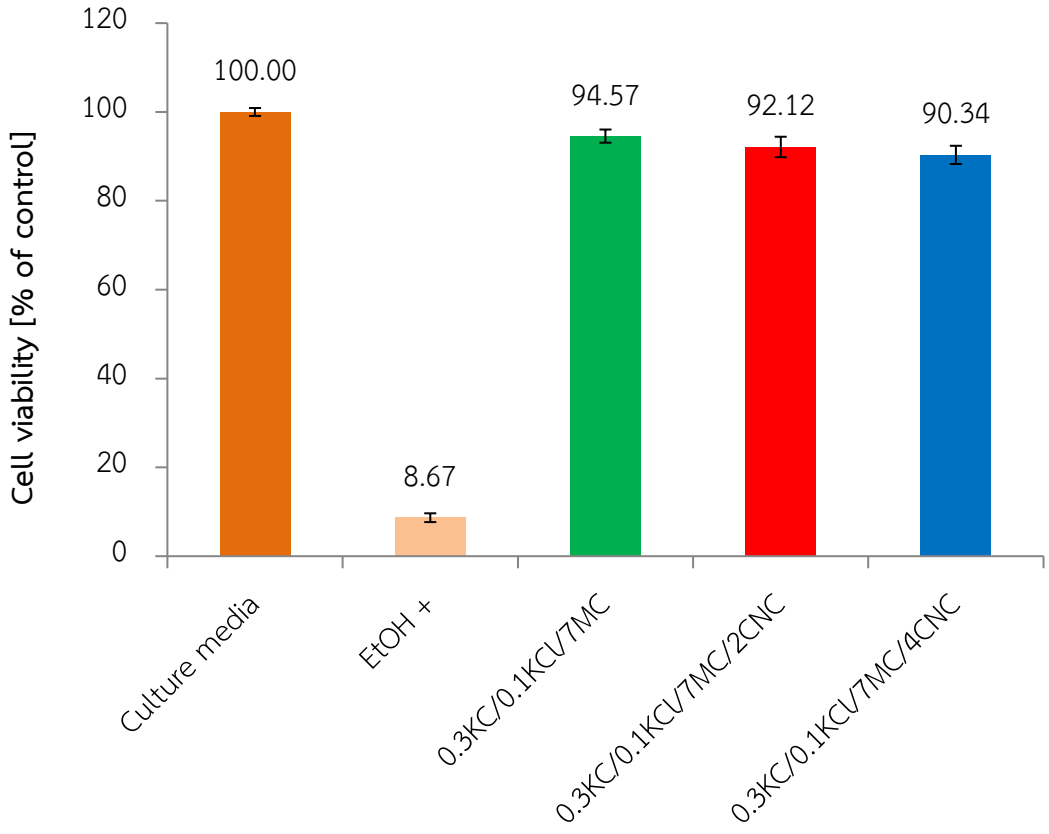

Figure 24. Percentage of cell viability of 0.3KC/0.1KCl/7MC, 0.3KC/0.1KCl/7MC/2CNC and 0.3KC/0.1KCl/7MC/4CNC hydrogels after incubation for 24 h.

4.1.8 Cell viability of bioprinting constructs

Cell viability of the bioprinted was evaluated using a live/dead cell-imaging assay, which was used to discriminate between live and dead cells at day 0, day 3 and day 5. The fluorescent images of the bioprinted 0.3KC/7MC/0.1KCl/2CNC and 0.3KC/7MC/0.1KCl/4CNC show the live (stained green), dead (stained red) as shown in Figure 25. The calcein generated from calcein-AM by esterase in the living cells emits green fluorescence in the cytoplasm, whereas the nuclei staining dye propidium iodide of dead cell emits red fluorescence (49, 107). On day 0, the cell viability of L929 cells in the 0.3KC/7MC/0.1KCl/2CNC and 0.3KC/7MC/0.1KCl/4CNC printed constructs was found to be 99.65 $\pm$ 0.12 and 99.79 $\pm$ 0.01 %, respectively, which was not statistically different from that of the control (99.65 $\pm$ 0.12%) ($p > 0.05$) as shown in Figure 26. This suggested that the bioprinted cell-laden materials and parameters engaged in this experiment did not have any toxic effect on the cells. Both bioprinted constructs exhibited cell viability greater than 90% on day 5, 0.3KC/7MC/0.1KCl/2CNC (92.70 $\pm$ 0.67%) and 0.3KC/7MC/0.1KCl/4CNC (90.60 $\pm$ 0.43%). Generally, these results clearly present that these two bioinks are biocompatible hydrogels and suitable for 3D bioprinting of living cells. These results combined with the cytotoxicity analysis clearly present that this bioink is a biocompatible hydrogel well suited for 3D bioprinting of living cells. In this work, small constructs were 3D bioprinted with cells.

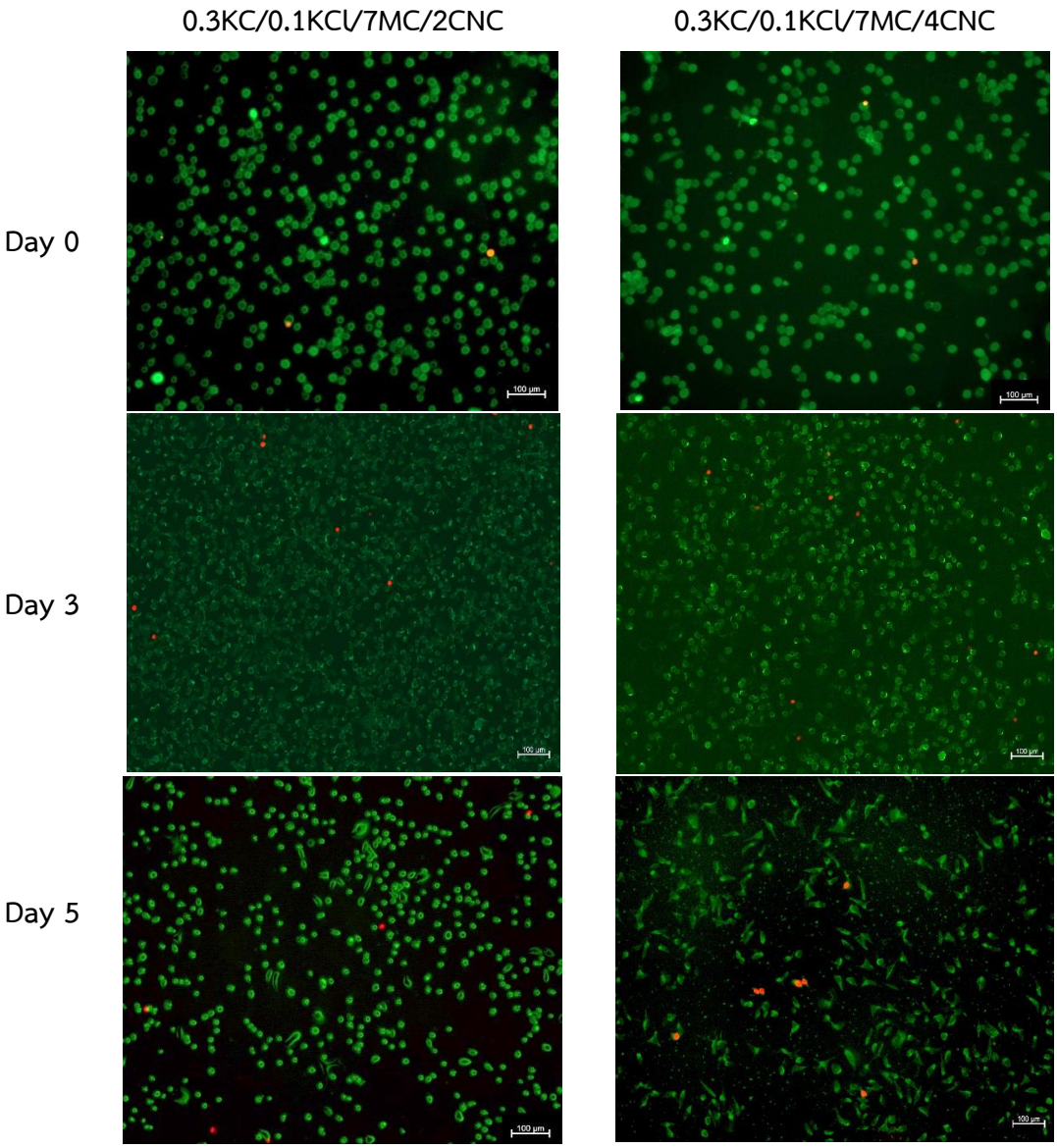

Figure 25. Merged live/ dead staining images of bioprinted 0. 3KC/ 0. 1KCl/ 7MC/ 2CNC and 0.3KC/0.1KCl/7MC/4CNC on days 0, 3 and 5 (scale bar, 100 μm).

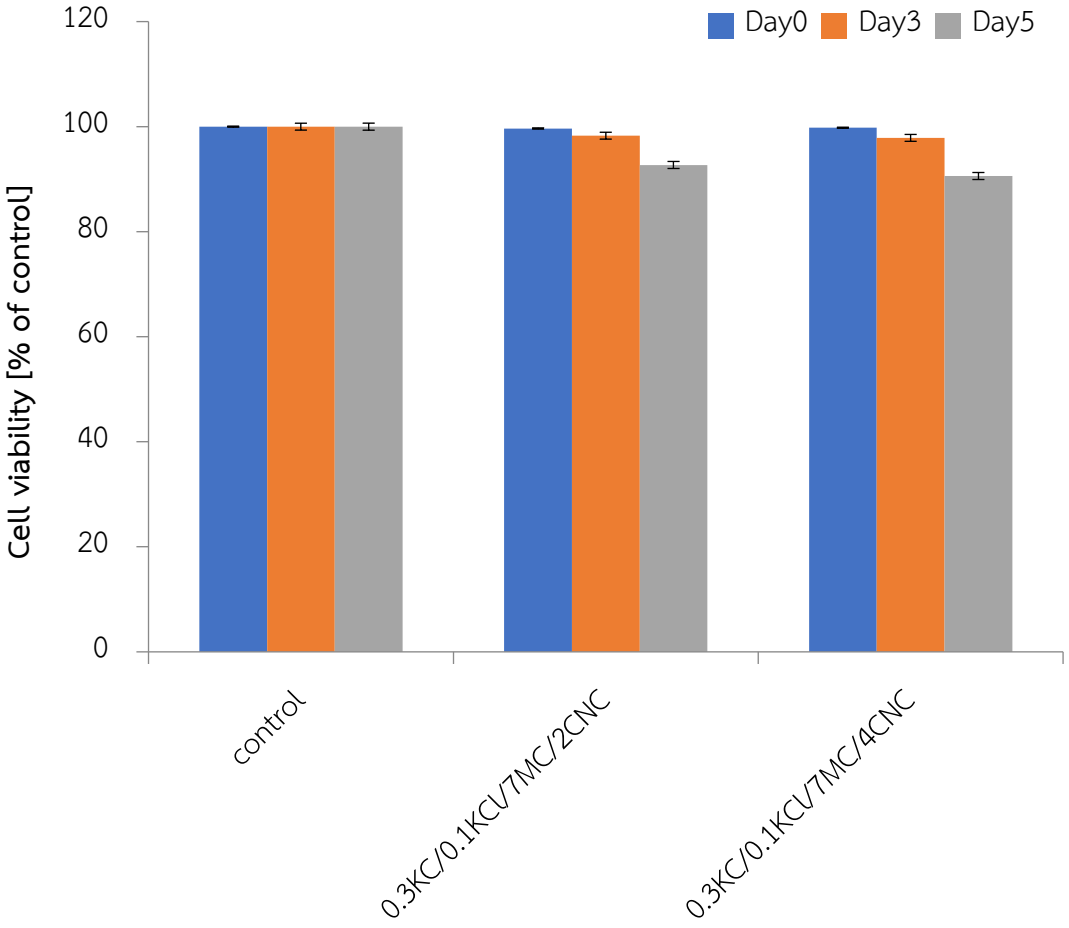

Figure 26. Cell viability on control and bioprinted 0.3KC/7MC/0.1KCl/2CNC and 0.3KC/0.1KCl/7MC/4CNC hydrogels.

4.2 PF/MC based hydrogels

4.2.1 Test tube tilting method (TTM) analysis

Based on test tube inversion results in Table 4.2, the mean values of the gelation temperature of 16PF was in a sol state at 4°C and room temperature (25 °C). 18PF, 20PF, and 22PF were in a sol state at 4°C and became soft gel at room temperature and body temperature (37 °C) (26). In addition, the mixture of 16PF/4MC was soft gel at 4 °C as well as 25°C and body temperatures. 18PF/4MC and 20PF/4MC were soft gel at room temperature but turned to gel at 37 °C, but 22PF/4MC became non-homogeneous. Therefore, the blends of 18PF/4MC and 20PF/4MC were further evaluated in the printing experiments.

Table 4.2 The gelation temperature (mean±SD, n=3) of the mixtures of PF and MC determined by the tube inversion method

Formulation	4°C	25°C	37°C
16PF	Sol	Sol	Soft gel
18PF	Sol	Soft gel	Soft gel
20PF	Sol	Soft gel	Soft gel
22PF	Sol	Soft gel	Soft gel
16PF/4MC	Soft gel	Soft gel	Soft gel
18PF/4MC	Soft gel	Soft gel	Stronger gel
20PF/4MC	Soft gel	Soft gel	Stronger gel
22PF/4MC	Non-homogeneous	Non-homogeneous	Non-homogeneous

4.2.2 Printability

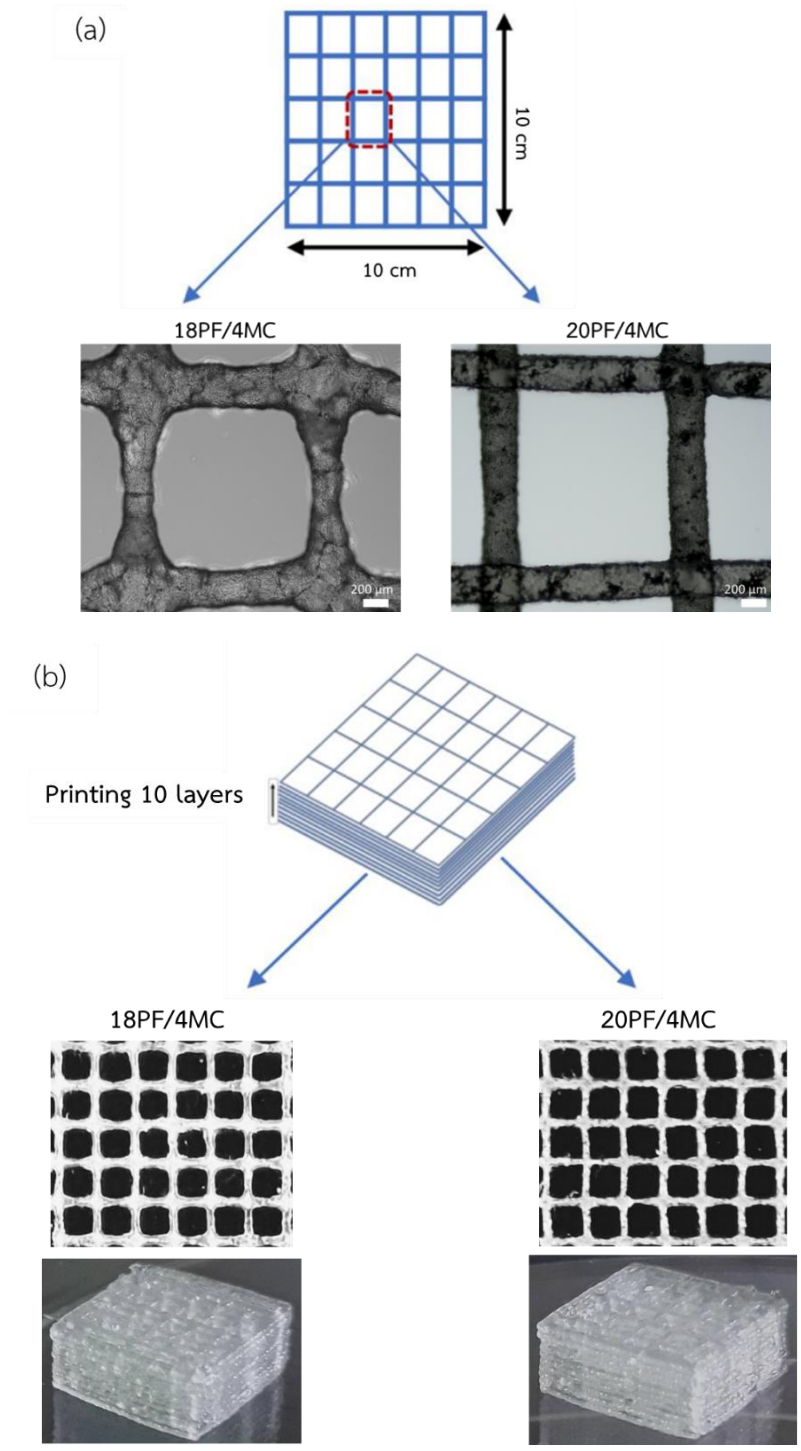

Figure 27. Optical microscopic (OM) images of the first layer of 18PF/4MC and 20PF/4MC bioprinted grid (scale bar, 200 µm) and (b) 3D-printed 10-layered structure of both 18PF/4MC and 20PF/4MC hydrogels.

As shown in Figure 27(a), 20PF/4MC showed excellent regularity with square holes but 18PF/4MC formed somewhat circular-like holes. The 3D structures of ten layers of both 18PF/4MC and 20PF/4MC are presented in Figure 27(b). The 20PF/4MC with higher concentration of PF exhibited a much higher printability than 18PF/4MC. These results indicated that increasing the concentration of PF resulted in more printability.

4.2.3 Rheological evaluation

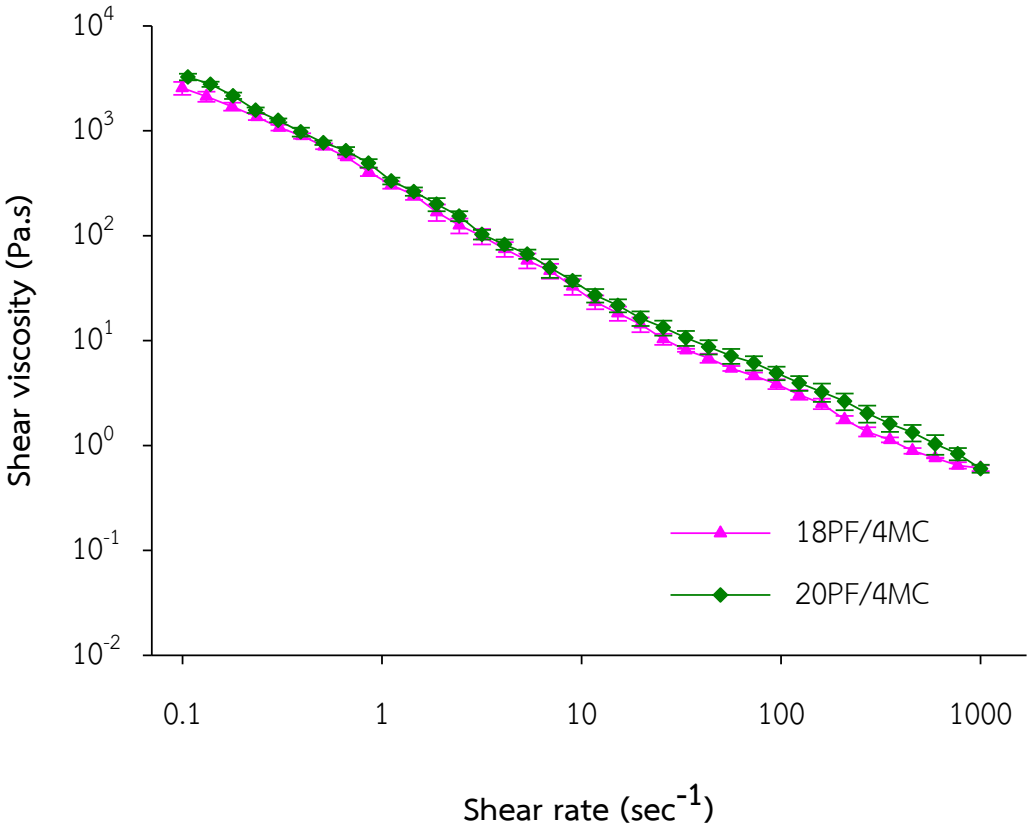

Figure 28. Rheological properties for 18PF/4MC and 20PF/4MC hydrogels at 25 °C: viscosity as a function of shear rate

As shown in Figure 28., viscosity of both 18PF/4MC and 20PF/4MC decreased as the shear rate increased. Both 18PF/4MC and 20PF/4MC yielded a confidence fit of $R^2 \geq 0.95$, R^2 values of the straight fitting lines of 18PF/4MC and 20PF/4MC were 0.9968 and 0.9966, respectively (97). For the mixture between PF and MC, increasing concentrations of PF in the blends resulted in an increase of the viscosity. The increase of the entanglements of the micelles as well as the interaction between PF and MC may link to the viscosity of the systems (26).

As shown in Figure 29., the viscosity of 18PF/4MC and 20PF/4MC recovered to 83.31% and 79.21% of the initial viscosity, respectively. Both hydrogels possessed the required characteristics (shear thinning and thixotropic) of a printable hydrogel for effective printing. However, based on printability experiment, 20PF/4MC showed better printability than 18PF/4MC.

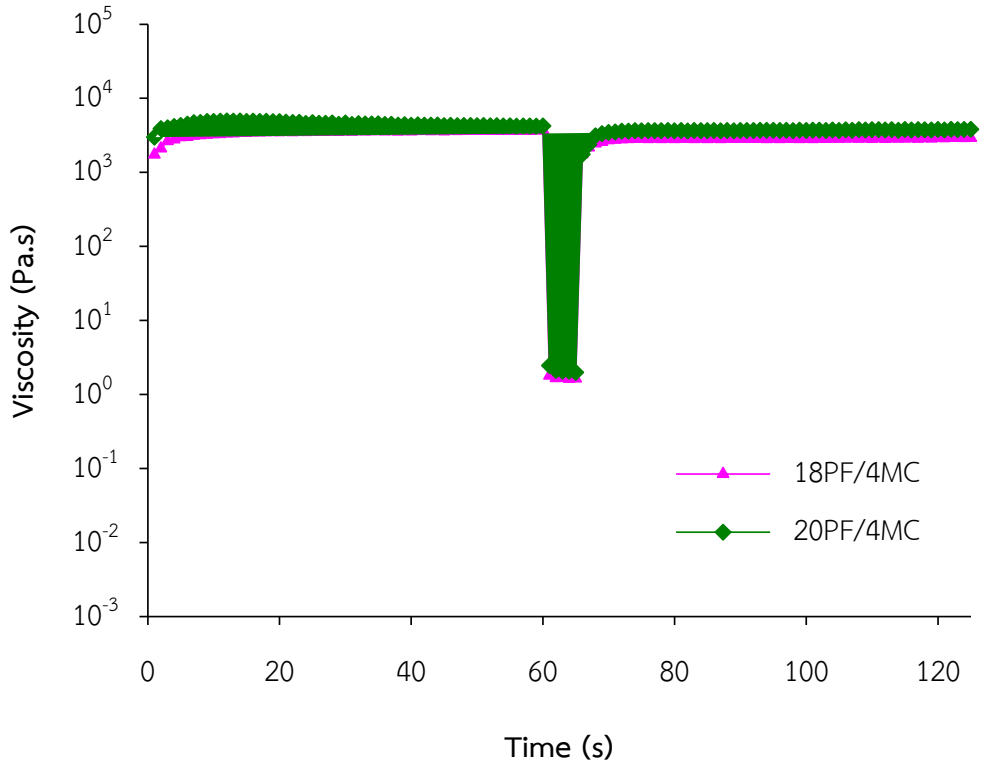

Figure 29. Recovery behavior of the hydrogels, the printing process simulated by the rheological study: step I, before printing; step II, during printing; and step III, after printing.

4.2.4 Morphological characterizations

All the samples were porous (Figure 30). The 18PF/4MC hydrogel displayed larger microsized pores of about 100 μm, Figure 30.(a-b). The mixtures of 20PF/4MC resulted in a lower porous microstructure. With higher content of PF (Figure 30.(c-d))., the pore size of 20PF/4MC decreased when compared to that of the 18PF/MC and indicated that a high amount of PF increased the compactness of the blend (26).

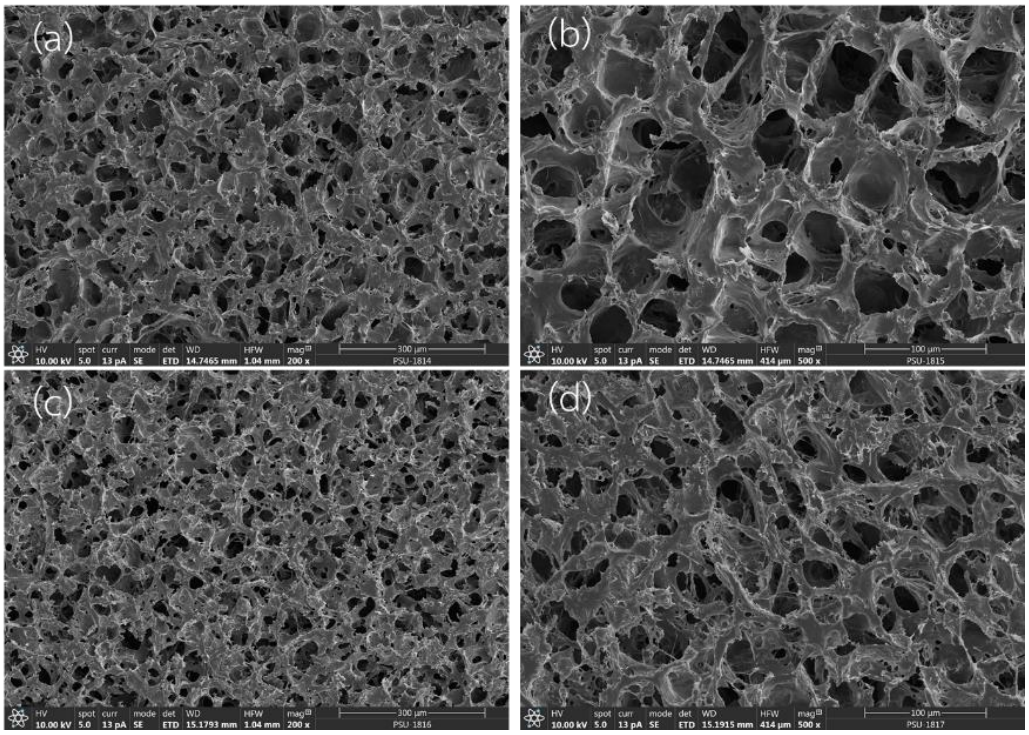

Figure 30. Scanning electron micrographs of freeze-dried (a-b) 18PF/4MC and (c-d) 20PF/4MC hydrogels.

4.2.5 Compression test

The strain-stress curves for 18PF/4MC and 20PF/4MC samples are shown in Figure 31. The compressive stress of 18PF, 20PF, 18PF/4MC and 20PF/4MC hydrogels was computed to be 2.42 ± 0.75, 3.05 ± 0.48, 17.10 ± 0.20 kPa and 18.76 ± 1.49 kPa, respectively (Figure 32.). Without the addition of MC, the 18PF, 20PF, hydrogel showed the least value. By adding MC, better compressive modulus was obtained. In addition, 18PF/4MC sample showed significantly lower compressive modulus than 20PF/4MC ($p < 0.001$). This suggested that the compressive modulus increased with increasing PF content, and PF was valuable for improving the mechanical strength of the samples.

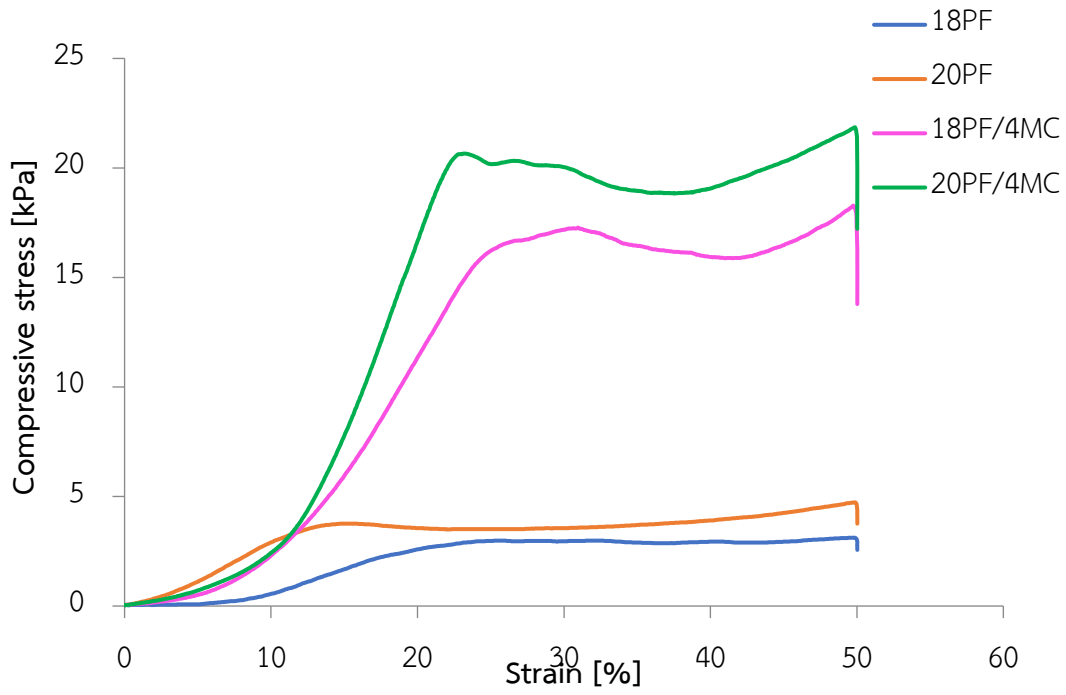

Figure 31. Compressive stress-strain curves for 18PF, 20PF, 18PF/4MC and 20PF/4MC hydrogels.

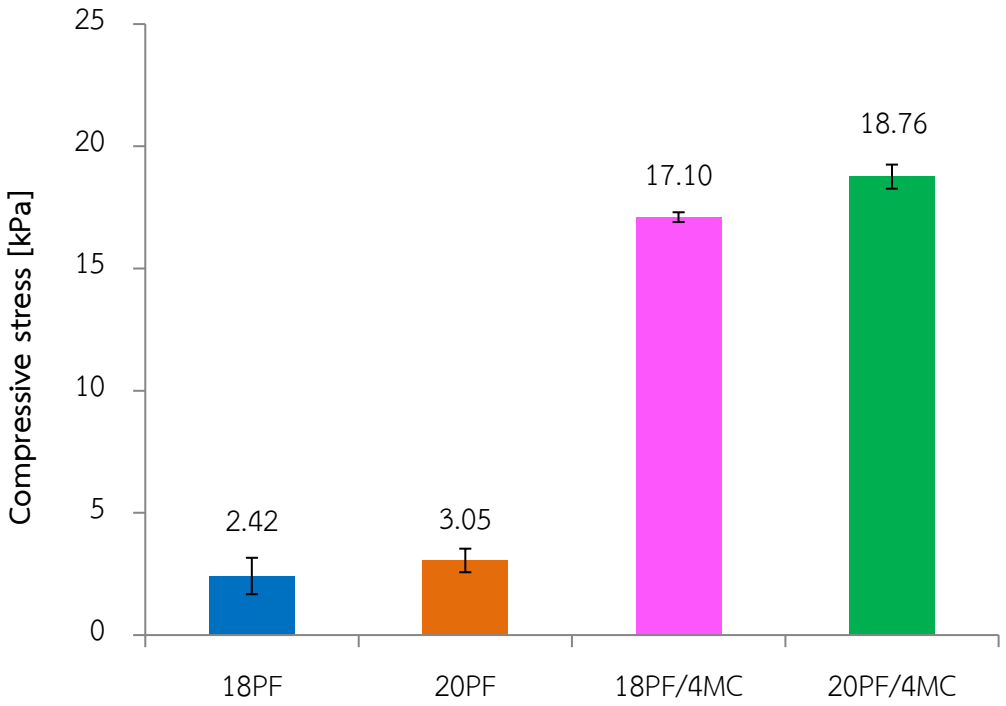

Figure 32. Compressive stress of 18PF, 20PF, 18PF/4MC and 20PF/4MC hydrogels.

4.2.6 Degradation of 18PF/4MC and 20PF/4MC hydrogels

The degradation of the hydrogels over time is presented in Figure 33. The weight loss of 18PF/4MC hydrogel at day 1, 4, 7, 14,21 and 30 was 101.33 ± 0.31, 99.69 ± 0.20, 79.38 ± 0.83, 51.32 ± 0.47, 42.58 ± 0.72 and 25.99 ± 0.43 %, respectively. Those of 20PF/4MC hydrogel at day 1, 4, 7, 14, 21 and 30 was 101.42 ± 0.57, 99.44 ± 0.44, 81.36 ± 0.50, 53.84 ± 0.58, 45.68 ± 0.80 and 29.61 ± 0.57 %, respectively. The degradation of the hydrogels over time is presented in Figure 33. Degradation of hydrogel with higher content of PF (20PF/4MC), was slightly lower than that with lower 18PF/ 4MC. In addition, the increase of viscosity in the system may retard the degradation as previously described (108). The viscosity at 25 °C of 20PF in the presence of MC (20PF/MC) increased. Therefore, the enhancement of viscosity might also delay the degradation of PF/MC (26).

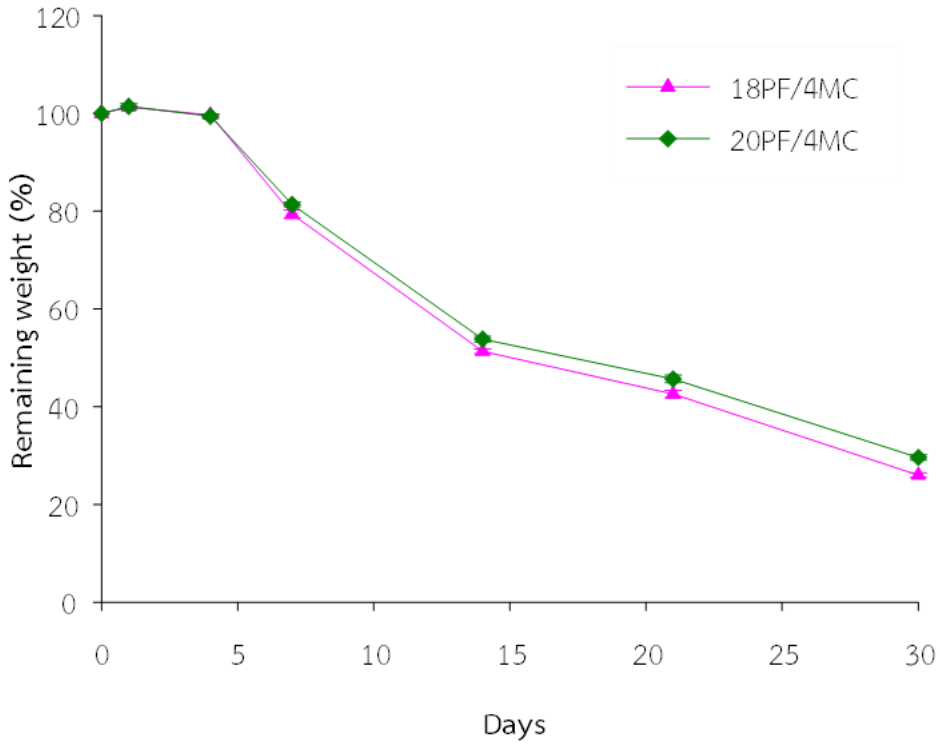

Figure 33. In vitro degradation of 18PF/4MC and 20PF/4MC hydrogels in deionized water at 37 °C.

4.2.7 Cytotoxicity analysis

The result of cytotoxicity assay is shown in Figure 34. Cell viability of the negative control (cell culture medium), positive control (ethanol), 18PF/4MC and 20PF/4MC was 100.0 ± 1.13%, 7.86 ± 1.14%, 98.56 ± 1.95% and 97.86 ± 1.07%, respectively. Cell viability of hydrogels was significantly different from each other ($p < 0.05$) and substantially lower than that of negative control ($p < 0.01$). However, the lower concentrations of PF domonstrated a slightly lower cytotoxicity than the high PF concentrations but were not statistically different.

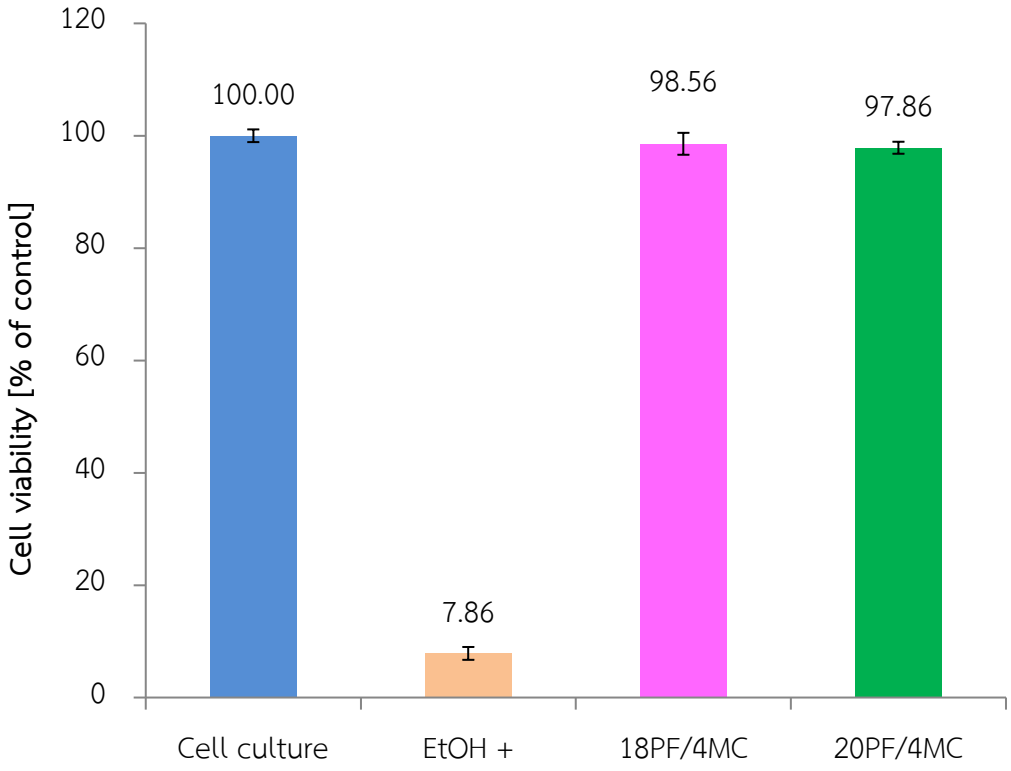

Figure 34. Percentage of cell viability of 18PF/4MC and 20PF/4MC hydrogels.

4.2.8 Cell viability of bioprinting constructs

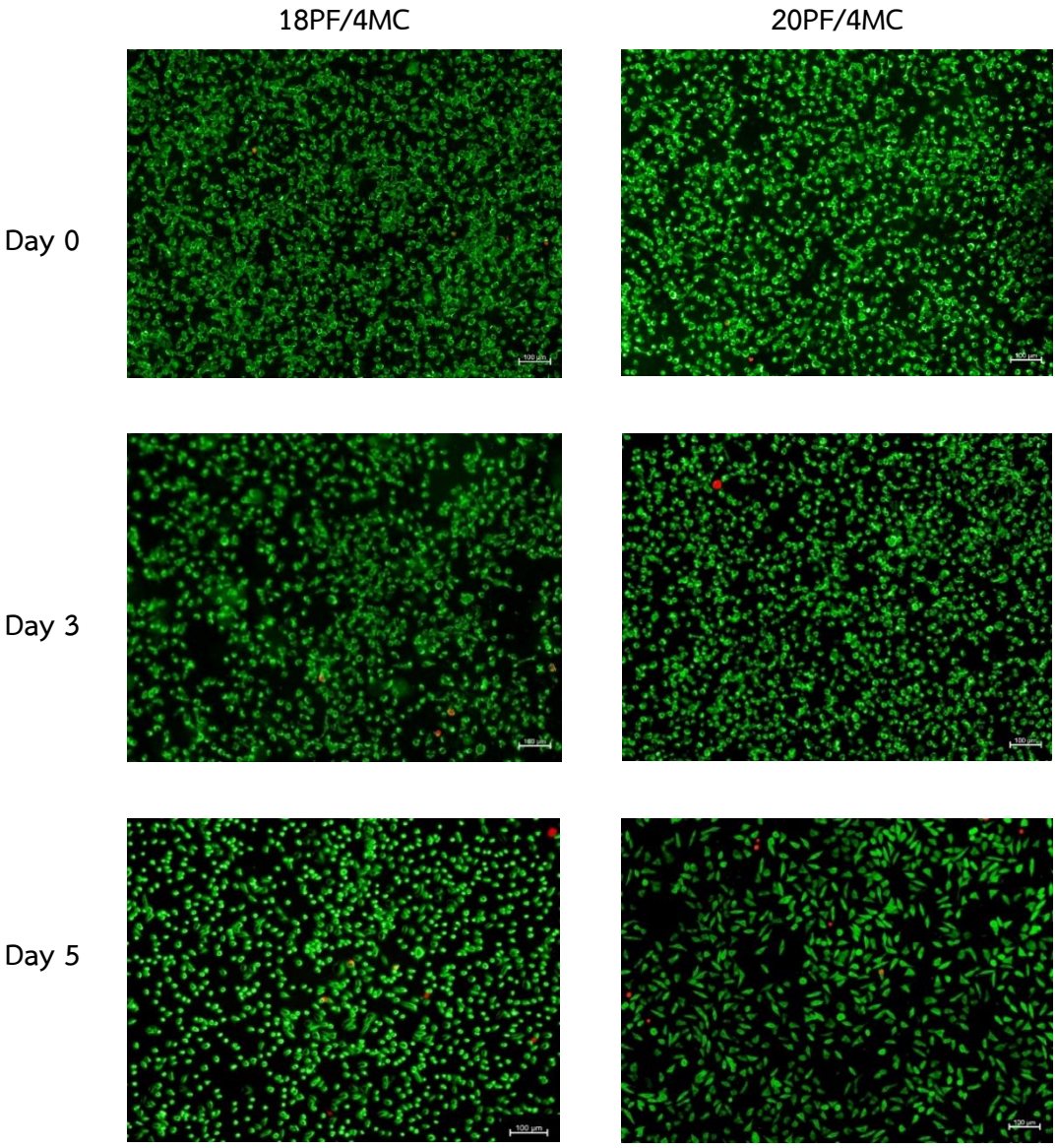

Figure 35. Merged live/dead staining images of bioprinted 18PF/4MC and 20PF/4MC on days 0, 3 and 5 (scale bar, 100 μm).

Cell viability of the bioprinted 18PF/4MC and 20PF/4MC was evaluated using a live/dead cell-imaging assay. The results are presented in Figure 35. The cell viability of L929 cells in the 18PF/4MC and 20PF/4MC printed constructs was found to be 99.64 ± 0.12% and 99.70 ± 0.01%, respectively, which was not statistically different from that of the control (99.71 ± 0.10%) on day 0 ($p > 0.05$) as shown in Figure 36. Both bioprinted constructs exhibited cell viability greater than 90% on day 5, 18PF/4MC (93.98 ± 0.67%) and 20PF/4MC (91.74 ± 0.43%). At day 5, almost all of the cells become elongated and highly spreading. These results clearly present that these two bioinks are biocompatible hydrogels and well-suited for 3D bioprinting of living cells. The PF/MC blends (18PF/4MC, 20PF/4MC) have increased compression modulus, which is the cause for increased cell viability, relative to the weaker blends (18PF, 20PF) (109).

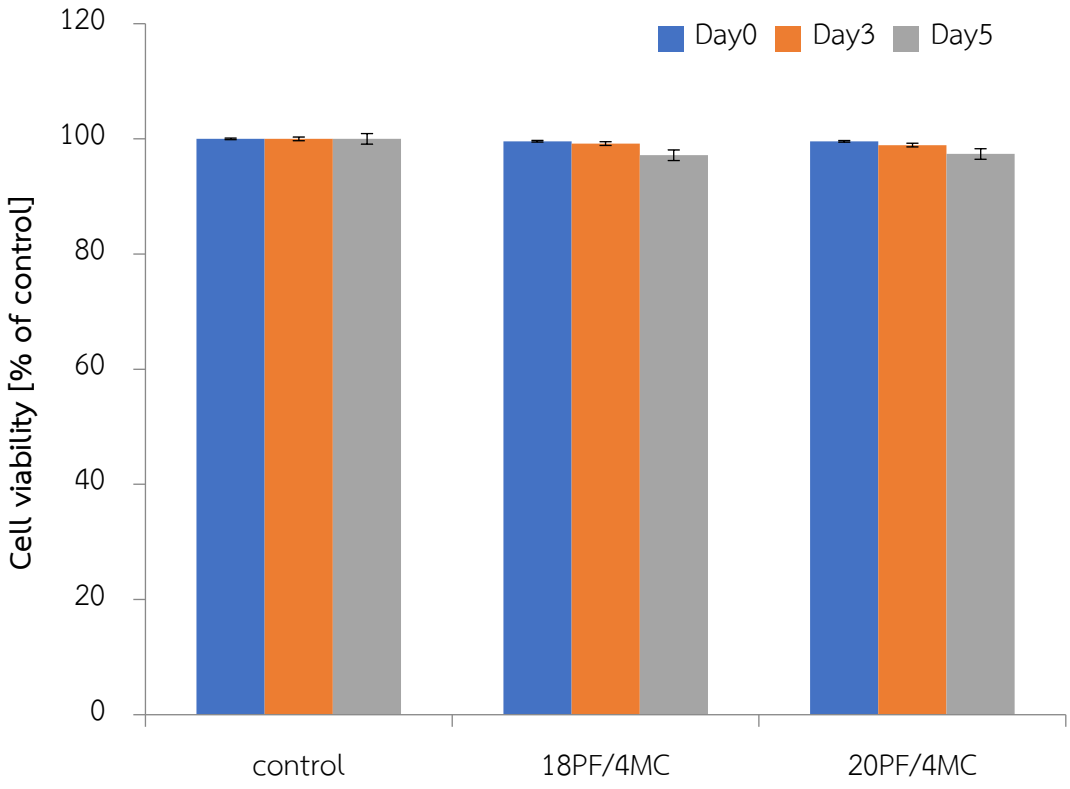

Figure 36. Cell viability on control and bioprinted 18PF/4MC and 20PF/4MC hydrogels.

CHAPTER 5

CONCLUSIONS

The properties that must be considered for bioprinting hydrogel are printability, biocompatibility, mechanical properties and shape/structure. For desirable printability, the hydrogels must possess suitable viscosity, viscoelasticity and shear-thinning property. The hydrogels must have suitable degradability, can be able to support cell attachments, cellular growth, cell proliferation and do not cause a serious adverse immune response or toxicity (110). The hydrogels should match the mechanical properties of targeting tissues in terms of strength, elasticity and stiffness (110). In addition, the printed construct should represent adequate similarity to the natural tissue in terms of structure and shape fidelity (110, 111).

The main objective of this study was to develop hydrogel-based bioinks, printability, mechanical properties and evaluate cell viability of the bioprinted constructs consisting of KC/MC and PF/MC. For KC/MC based system, the hydrogel with high content of CNC, 0.3KC/0.1KCl/7MC/4CNC, exhibited good thixotropic behavior than 0.3KC/0.1KCl/7MC/2CNC. The 0.3KC/0.1KCl/7MC/4CNC hydrogel hydrogel exhibited slightly better printability than 0.3KC/0.1KCl/7MC/2CNC. In addition, FE-SEM, the pore sizes decreased in the order of 0.3KC/0.1KCl/7MC > 0.3KC/0.1KCl/7MC/2CNC > 0.3KC/0.1KCl/7MC/4CNC. Compressive mechanical strength was significantly higher in the presence of CNC; and higher CNC concentrations exhibited higher mechanical strength (0.3KC/0.1KCl/7MC/4CNC > 0.3KC/0.1KCl/7MC/2CNC). The weight loss of of 0.3KC/0.1KCl/7MC/2CNC was slightly lower than that of 0.3KC/0.1KCl/7MC/4CNC with about 86 - 89 % degradation within 30 days. Based on indirect cytotoxicity MTT assay, cell viability was slightly lower in the presence of CNC compared to that without CNC. Nevertheless, the blend of 0.3KC/0.1KCl/7MC/4CNC and 0.3KC/0.1KCl/7MC/2CNC showed good cell viability (> 90%). Both 0.3KC/0.1KCl/7MC/2CNC and 0.3KC/0.1KCl/7MC/4CNC bioprinted constructs exhibited cell viability greater than 90% on day 5.

Regarding PF/MC based system, the blends of 18PF/4MC and 20PF/4MC exhibited good thixotropic behavior. Then high PF concentration of 20PF/MC showed better shear-thinning behavior than 18PF/MC. The 20PF/4MC hydrogel exhibited slightly better printability than 18PF/4MC. According to FE-SEM, the pore sizes of 18PF/4MC were bigger than that of 20PF/MC blends so the presence of PF enhanced the compactness of the blends. The compressive mechanical strength was significantly higher PF concentrations exhibited higher mechanical strength (20PF/4MC > 18PF/4MC). The weight loss of of 18PF/4MC was slightly lower than that of 20PF/4MC with about 71 - 74 % degradation within a month. However, all hydrogels presented cell viability above 90%, demonstrating good biocompatibility. Thus, both the 20PF/4MC and 18PF/4MC bioprinted constructs exhibited cell viability greater than 90% on day 5.

The pore size of 20PF/MC was smaller than that of 0.3KC/7MC/0.1KCl/4CNC. In addition, 20PF/MC sample showed lower compressive stress than 0.3KC/0.1KCl/7MC/4CNC. The results from the indirect cytotoxicity test and cell viability analysis of 0.3KC/7MC/0.1KCl/4CNC and 20PF/MC for 3D printed bioink with L929 showed that the tested bioink is biocompatible and suitable for cell culture. Degradation of 20PF/MC was slightly lower than 0.3KC/7MC/0.1KCl/4CNC. All of the tested hydrogels exhibited a thixotropic property. Therefore, the blend 20PF/4MC and 0.3KC/0.1KCl/7MC/4CNC are particularly suited to cell-encapsulated 3D bioprinting applications.

REFERENCES

1. I. Diañez, C. Gallegos, Fuente EB-dl, Martínez I, C. Valencia, M.C. Sánchez, et al. 3D printing in situ gelification of K-carrageenan solutions: Effect of printing variables on the rheological response. Food Hydrocolloids. 2019;87:321-30.
2. Jones N. Three-dimensional printers are opening up new worlds to research. Nature. 2012;487(7405):22-3.
3. He Y, Yang FF, Zhao HM, Gao Q, Xia B, Fu JZ. Research on the printability of hydrogels in 3D bioprinting. Scientific Reports. 2016;6.
4. Wang S, Lee JM, Yeong WY. Smart hydrogels for 3D bioprinting. International Journal of Bioprinting. 2015;1(1).
5. PA G, R. A. Biodegradable synthetic polymers for tissue engineering. European cells & materials. 2003;20;5:1-16.
6. Malafaya PB, Silva GA, Reis RL. Natural-origin polymers as carriers and scaffolds for biomolecules and cell delivery in tissue engineering applications. Advanced Drug Delivery Reviews. 2007;30;59(4-5):207-33.
7. Wu ZJ, Su X, Xu YY, Kong B, Sun W, Mi SL. Bioprinting three-dimensional cell-laden tissue constructs with controllable degradation. Scientific Reports. 2016;6.
8. Li H, Liu S, Li L. Rheological study on 3D printability of alginate hydrogel and effect of graphene oxide. International Journal of Bioprinting. 2016;2(2):54-66.
9. Ouyang L, Highley CB, Rodell CB, Sun W, Burdick JA. 3D Printing of shear-thinning hyaluronic acid hydrogels with secondary cross-linking. American Chemical Society Biomaterials Science & Engineering 2016;2(10):1743-51
10. Sundaramurthi D, Rauf S, Hauser CAE. 3D bioprinting technology for regenerative medicine applications. International Journal of Bioprinting. 2016;2(2):9-26.
11. Malda J, Visser J, Melchels FP, Jungst T, Hennink WE, Dhert WJA, et al. 25th Anniversary article: engineering hydrogels for biofabrication. Advanced Materials. 2013;25(36):5011-28.

12. Wu D, Yu Y, Tan J, Huang L, Luo B, Lu L, et al. 3D bioprinting of gellan gum and poly (ethylene glycol) diacrylate based hydrogels to produce human-scale constructs with high-fidelity. Materials & Design. 2018;160:486-95.
13. Naghieh S, Sarker MD, Abelseth E, Chen X. Indirect 3D bioprinting and characterization of alginate scaffolds for potential nerve tissue engineering applications. Journal of the Mechanical Behavior of Biomedical Materials. 2019;93:183-93.
14. Malda J, Visser J, Melchels FP, Jungst T, Hennink WE, Dhert WJA, et al. 25th Anniversary article: engineering hydrogels for biofabrication. Advanced Materials. 2013;25(36):5011-28.
15. Li HJ, Tan YJ, Leong KF, Li L. 3D Bioprinting of highly thixotropic alginate/methylcellulose hydrogel with strong interface bonding. ACS Applied Materials & Interfaces. 2017;9(23):20086-97.
16. Guvendiren M, Lu HD, Burdick JA. Shear-thinning hydrogels for biomedical applications. Soft Matter. 2012;8(2):260-72.
17. Loebel C, Rodell CB, Chen MH, Burdick JA. Shear-thinning and self-healing hydrogels as injectable therapeutics and for 3D-printing. Nature Protocols. 2017;12(8):1521-41.
18. Skardal A, Atala A. Biomaterials for integration with 3-D bioprinting. Annals of Biomedical Engineering. 2015;43(3):730-46.
19. Billiet T, Vandenhaute M, Schelfhout J, Van Vlierberghe S, Dubruel P. A review of trends and limitations in hydrogel-rapid prototyping for tissue engineering. Biomaterials. 2012;33(26):6020-41.
20. Tan YJ, Tan XP, Yeong WY, Tor SB. Hybrid microscaffold-based 3D bioprinting of multi-cellular constructs with high compressive strength: A new biofabrication strategy. Scientific Reports. 2016;6.
21. Cui X, KB, MGF, Martin Lotz, DDDL. Direct human cartilage repair using three-dimensional bioprinting technology. Tissue Engineering Part A. 2012 11-12:1304-12.

22. Fedorovich NE, JRDW, AJV, JA, WJAD. Three-dimensional fiber deposition of cell-laden, viable, patterned constructs for bone tissue printing. Tissue Engineering Part A. 2008;14:127-33.
23. Jia W, Gungor-Ozkerim PS, Zhang YS, Yue K, Zhu K, Liu W, et al. Direct 3D bioprinting of perfusable vascular constructs using a blend bioink. Biomaterials. 2016;106:58-68.
24. Wang X, QA, XT, JF, HT, WH, et al. Gelatin-Based hydrogels for organ 3D bioprinting. Polymers. 2017;9.
25. Das S, FP, Y-JC, GR, J-HS, SWK, et al. Bioprintable, cell-laden silk fibroin-gelatin hydrogel supporting multilineage differentiation of stem cells for fabrication of three-dimensional tissue constructs. Acta Biomaterialia. 2015;11:233-46.
26. Rangabhatla ASL, Tantishaiyakul V, Oungbho K, Boonrat O. Fabrication of pluronic and methylcellulose for etidronate delivery and their application for osteogenesis. International Journal of Pharmaceutics. 2016;499(1-2):110-8.
27. Kuchler RJ, Marlowe ML, Merchant DJ. The mechanism of cell binding and cell-sheet formation in L strain fibroblasts. Experimental Cell Research. 1960;20(2):428-37.
28. Sangfai T, Tantishaiyakul V, Hirun N, Li L. Microphase Separation and Gelation of Methylcellulose in the Presence of Gallic Acid and NaCl as an In Situ Gel-Forming Drug Delivery System. AAPS PharmsciTech. 2017;18(3):605-16.
29. Tecante A, Núñez SMdC. Solution properties of KC and its interaction with other polysaccharides in aqueous media.pdf. InTech ISBN: 978-953-51-0187-1. 2012:241–64.
30. Liu Z, Bhandari B, Prakash S, Mantihal S, Zhang M. Linking rheology and printability of a multicomponent gel system of carrageenan-xanthan-starch in extrusion based additive manufacturing. Food Hydrocolloids. 2019;87:413-24.
31. Kim MH, Kim BS, Park H, Lee J, Park WH. Injectable methylcellulose hydrogel containing calcium phosphate nanoparticles for bone regeneration. International Journal of Biological Macromolecules. 2018;109:57-64.

32. Li H, Tan C, Li L. Review of 3D printable hydrogels and constructs. Materials and Design 2018;159:20–38.
33. Gao GF, Cui XF. Three-dimensional bioprinting in tissue engineering and regenerative medicine. Biotechnology Letters. 2016;38(2):203-11.
34. Jones N. Three-dimensional printers are opening up new worlds to research. Nature 2012;487(7405):22-3.
35. Ning LQ, Chen XB. A brief review of extrusion-based tissue scaffold bio-printing. Biotechnology Journal. 2017;12(8).
36. Murphy SV, Atala A. 3D bioprinting of tissues and organs. nature biotechnology. 2014;32:773-85.
37. Nahmias Y, Schwartz RE, Verfaillie CM, Odde DJ. Laser-guided direct writing for three-dimensional tissue engineering. Biotechnology and Bioengineering. 2005;92(2):129-36.
38. Xu T, Jin J, Gregory C, Hickman JJ, Boland T. Inkjet printing of viable mammalian cells. Biomaterials. 2005;26(1):93-9.
39. Faulkner-Jones A, Greenhough S, King JA, Gardner J, Courtney A, Shu WM. Development of a valve-based cell printer for the formation of human embryonic stem cell spheroid aggregates. Biofabrication. 2013;5(1).
40. Yan YN, Wang XH, Pan YQ, Liu HX, Cheng J, Xiong Z, et al. Fabrication of viable tissue-engineered constructs with 3D cell-assembly technique. Biomaterials. 2005;26(29):5864-71.
41. Ward MA, Georgiou TK. Thermoresponsive Polymers for Biomedical Applications Polymers. polymers. 2011;3:1215-42.
42. Lee M, KB, PG, JC, ØA, MZ-W. Exploitation of Cationic Silica Nanoparticles for Bioprinting of Large-Scale Constructs with High Printing Fidelity. ACS Appl Mater Interfaces 2018;10 (44) 37820–8.
43. Bendtsen ST, SPQ, MW. Development of a novel alginate-polyvinyl alcohol-hydroxyapatite hydrogel for 3D bioprinting bone tissue engineered scaffolds. Journal of Biomedical Materials Research. 2017 105(5):1457-68.
44. Fan Y, TS, XY, FS, DY. 3D Composite Cell Printing Gelatin/Sodium Alginate/n-HAP Bioscaffold Journal of Physics: Conf Series 1213 2019;4:042020.

45. Chimene D, CWP, JLG, JKC, LMC, EM, et al. Nanoengineered Ionic–Covalent Entanglement (NICE) Bioinks for 3D Bioprinting. ACS Applied Materials & I nterfaces. 2018;10:9957–68.
46. Demirtaş TT, GI, MG. A bioprintable form of chitosan hydrogel for bone tissue engineering. Biofabrication 2017 9 035003.
47. Ahlfeld T, GC, DK, SD, ARA, JID, et al. Development of a clay based bioink for 3D cell printing for skeletal application. Biofabrication. 2017;9(3):034103.
48. Suntornnond R, EYST, JA, CKC. A highly printable and biocompatible hydrogel composite for direct printing of soft and perfusable vasculature-like structures. Scientific Reports. 2017;7:16902.
49. Markstedt K, Mantas A, Tournier I, Ávila HM, Hägg D, Gatenholm P. 3D bioprinting human chondrocytes with nanocellulose–alginate bioink for cartilage tissue engineering applications. Biomacromolecules 2015;16:1489–96.
50. Giuseppe MD, Law N, Webb B, A. Macrae R, Liew LJ, Sercombe TB, et al. Mechanical behaviour of alginate-gelatin hydrogels for 3D bioprinting. Journal of the Mechanical Behavior of Biomedical Materials. 2018;79:150-7.
51. Li H, Tan YJ, Li L. A strategy for strong interface bonding by 3D bioprinting of oppositely charged K-carrageenan and gelatin hydrogels. Carbohydrate Polymers. 2018;198:261-9.
52. Wu Y, Lin ZY, Wenger AC, Tam KC, Tang X. 3D bioprinting of liver-mimetic construct with alginate/cellulose nanocrystal hybrid bioink. Bioprinting. 2018;9:1-6.
53. Chawla S, AK, PA, AB, SG. Elucidating role of silk-gelatin bioink to recapitulate articular cartilage differentiation in 3D bioprinted constructs. Bioprinting 2017;7:1–13.
54. Narayanan LK, PH, MBF, JTS, BS, RAS. 3D-Bioprinting of Polylactic Acid (PLA) Nanofiber–Alginate Hydrogel Bioink Containing Human Adipose-Derived Stem Cells. ACS Biomaterials Science & Engineering. 2016;2:1732–42.
55. Pillay V, Seedat, A., Choonara, Y. E., Toit, L. C. d., Kumar, P., & Ndesendo, V. M. K. . A review of polymeric refabrication techniques to modify polymer

properties for biomedical and drug delivery applications. Journal of the American Association of Pharmaceutical Scientists. 2013;14(2:692-711.

56. Strandman S, XXZ. Thermo-responsive block copolymers with multiple phase transition temperatures in aqueous solutions. Progress in Polymer Science. 2015;42:154-76.

57. Gandhi A, Abhijit Paul, Sen SO, Sen KK. Studies on thermoresponsive polymers: phase behaviour, drug delivery and biomedical applications. . Asian journal of pharmaceutical sciences. 2015;10:99 -107.

58. Bajpai AK, SKS, SB, SK. Responsive polymers in controlled drug delivery. Progress in Polymer Science. 2008;33:1088-118.

59. Tomšicˇ M, Prossnigg F, Glatter O. A thermoreversible double gel: Characterization of a methylcellulose and K-carrageenan mixed system in water by SAXS, DSC and rheology. Journal of Colloid and Interface Science. 2008;322:41–50.

60. Mangione MR, Giacomazza D, Bulone D, Martorana V, Cavallaro G, Biagio PLS. K^+ and Na^+ effects on the gelation properties of n-Carrageenan. Biophysical Chemistry 2005;113:129 – 35.

61. Nalinda A, Leela R, Jin Z. The effect of kappa carrageenan and salt on thermoreversible gelation of methylcellulose. Polymer Bulletin. 2018;75:4227–43.

62. Liu J, Zhan X, Wan J, Wang Y, Wang C. Review for carrageenan-based pharmaceutical biomaterials: favourable physical features versus adverse biological effects. Carbohydrate Polymers. 2015;121:27-36.

63. Wang Y, Yuan C, Cui B, Liu Y. Influence of cations on texture, compressive elastic modulus, sol-gel transition and freeze-thaw properties of kappa-carrageenan gel. Carbohydrate Polymers. 2018;202:530-5.

64. Ahlfeld T, Köhler T, Czichy C, Lode A, Gelinsky M. A Methylcellulose Hydrogel as Support for 3D Plotting of Complex Shaped Calcium Phosphate Scaffolds. Gels. 2018;4(3):68.

65. Boonrat O, VT, NH. Micellization and gelation characteristics of different blends of pluronic F127/methylcellulose and their use as mucoadhesive in situ gel for periodontitis. Polym Bull. 2021;78:1175-87.
66. Park H, Kim MH, Yoon YI, Park WH. One-pot synthesis of injectable methylcellulose hydrogel containing calcium phosphate nanoparticles. Carbohydrate Polymers 2017;157:775–83.
67. Bhowmick B, Sarkar G, Rana D, Roy I, Saha NR, Ghosh S, et al. Effect of carrageenan and potassium chloride on an in situ gelling ophthalmic drug delivery system based on methylcellulose. RSC Advances. 2015;5:60386–91.
68. Yin Z, Wu F, Xing T, Yadavalli VK, Kundu SC, Lu S. A silk fibroin hydrogel with reversible sol-gel transition. Rsc Advances. 2017;7(39):24085-96
69. George J, Sabapathi S. Cellulose nanocrystals: synthesis, functional properties, and applications. Nanotechnology Science and Applications. 2015;8:45–54.
70. Curvello R, Singh V, GilGarnier R. Engineering nanocellulose hydrogels for biomedical applications. Advances in Colloid and Interface Science. 2019;267:47-61.
71. Kopeček J. Smart and genetically engineered biomaterials and drug delivery systems. European Journal of Pharmaceutical Sciences 2003;20:1-16.
72. Matanović MR, Kristl J, Grabnar PA. Thermoresponsive polymers: Insights into decisive hydrogel characteristics, mechanisms of gelation, and promising biomedical applications. International Journal of Pharmaceutics 2014;472:262-75.
73. Liu T, Chu B. Formation of homogeneous gel-like phases by mixed triblock copolymer micelles in aqueous solution: FCC to BCC phase transition. Journal of Applied Crystallography. 2000;33:727-30.
74. Sharma PK, Reilly MJ, Bhatia SK, Sakhitab N, Archambault JD, Bhatia SR. Effect of pharmaceuticals on thermoreversible gelation of PEO–PPO–PEO copolymers. Colloids and Surfaces B: Biointerfaces 2008;63:229-35.
75. Choi H-G, Lee M-K, Kim M-H, Kim C-K. Effect of additives on the physicochemical properties of liquid suppository bases. International Journal of Pharmaceutics 1999;190:13-9.

76. Yong CS, Choi JS, Quan Q-Z, Rhee J-D, Kim C-K, Lim S-J, et al. Effect of sodium chloride on the gelation temperature, gel strength and bioadhesive force of poloxamer gels containing diclofenac sodium. Int J Pharm. 2001;226(1-2):195-205.

77. Yong CS, Choi JS, Quan Q-Z, lRhee J-D, Kim C-K, Lim S-J, et al. Effect of sodium chloride on the gelation temperature, gel strength and bioadhesive force of poloxamer gels containing diclofenac sodium. International Journal of Pharmaceutics. 2001;226(1-2):195-205.

78. Dumortier G, Grossiord JL, Agnely F, Chaumeil JC. A Review of Poloxamer 407 Pharmaceutical and Pharmacological Characteristics. Pharmaceutical Research. 2006;23(12):2709-28.

79. Sangfai T, Tantishaiyakul V, Hirun N, Li L. Preparation and characterization of **K**-carrageenan and xyloglucan blends for sustained release of a hydrophilic drug. Polymer Bulletin. 2015;72(7):1647-61.

80. Wang Q, Li L, Liu E, Xu Y, Liu J. Effects of SDS on the sol–gel transition of methylcellulose in water. Polymer. 2006;47(4):1372-8.

81. Boonlai W, Tantishaiyakul V, Hirun N, Sangfai T, Suknuntha K. Thermosensitive Poloxamer 407/Poly(Acrylic Acid) Hydrogels with Potential Application as Injectable Drug Delivery System. AAPS PharmSciTech. 2018.

82. Martin BC, Minner EJ, Wiseman SL, Klank RL, Gilbert RJ. Agarose and methylcellulose hydrogel blends for nerve regeneration applications. Journal of Neural Engineering. 2008;5(2):221-31.

83. Yap L-S, Yang M-C. Evaluation of hydrogel composing of Pluronic F127 and carboxymethyl hexanoyl chitosan as injectable scaffold for tissue engineering applications. Colloids and Surfaces B: Biointerfaces 2016;146:204–11.

84. Khodaverdi E, Tafaghodi M, Ganji F, Abnoos K, Naghizadeh H. In Vitro Insulin Release from Thermosensitive Chitosan Hydrogel. AAPS PharmSciTech. 2012;13(2):460-6.

85. Boonrat O, VT, NH, SR, SS. Structural characterization using SAXS and rheological behaviors of pluronic F127 and methylcellulose blends. Polymer Bulletin 2021;78:1175–87.

86. Li H, Tan YJ, Leong KF, Li L. 3D Bioprinting of Highly Thixotropic Alginate/Methylcellulose Hydrogel with Strong Interface Bonding. ACS Applied Materials & Interfaces. 2017;9(23):20086-97.
87. Li H, Tan YJ, Liu S, Li L. Three-Dimensional Bioprinting of Oppositely Charged Hydrogels with Super Strong Interface Bonding. ACS Applied Materials & Interfaces. 2018;10(13):11164-74.
88. Biological Reactivity Tests In Vitro. USP42-NF37 (87). Interim Revision Announcement. 2015.
89. Jamuna-Thevi K, Bakar SA, Ibrahim S, Shahab N, Toff MRM. Quantification of silver ion release, in vitro cytotoxicity and antibacterial properties of nanostuctured Ag doped TiO2 coatings on stainless steel deposited by RF magnetron sputtering. 86 2011:235-41.
90. Gong H, Zhang X, Cheng B, Sun Y, Li C, Li T, et al. Bisphenol A Accelerates Toxic Amyloid Formation of Human Islet Amyloid Polypeptide: A Possible Link between Bisphenol A Exposure and Type 2 Diabetes. PLoS One. 2013;8(1):54198.
91. Le T-D, Do TAT, Yu R, Yoo H. Ethanol Elicits Inhibitory Effect on the Growth and Proliferation of Tongue Carcinoma Cells by Inducing Cell Cycle Arrest. Korean J Physiol Pharmacol. 2012;16:153-8.
92. Boonlai W, Tantishaiyakul V, Hirun N. Characterization of K-carrageenan/methylcellulose/cellulose nanocrystal hydrogels for 3D bioprinting. Polymer International. 2022;71:181–91.
93. Bhowmik M, MKB, LKG, DC. Effect of salts on gelation and drug release profiles of methylcellulose-based ophthalmic thermo-reversible in situ gels. Pharmaceutical Development and Technology. 2011 16:385-91.
94. Xu Y, LL, PZ, YCL, XH. Controllable Gelation of Methylcellulose by a Salt Mixture. Langmuir 2004;20:6134-8.
95. Shariatnia S, AVK, OK, AA. Hybrid Cellulose Nanocrystal-Bonded Carbon Nanotubes/Carbon Fiber Polymer Composites for Structural Applications. ACS Applied Nano Materials. 2020;3:5421–36.

96. Ouyang L, Yao R, Zhao Y, Sun W. Effect of bioink properties on printability and cell viability for 3D bioplotting of embryonic stem cells. Biofabrication. 2016; 8 035020.

97. Rodriguez MJ, Brown J, Giordano J, Lin SJ, Omenetto FG, Kaplan DL. Silk Based Bioinks for Soft Tissue Reconstruction Using 3-Dimensional (3D) Printing with in vitro and in vivo Assessments. Biomaterials 2017;117:105-15.

98. Wilson SA, Cross LM, Peak CW, Gaharwar AK. Shear-thinning and thermo-reversible nanoengineered inks for 3d bioprinting. ACS Appl Mater Interfaces. 2017;9(50):43449-58.

99. Bhandari PN, Singhal RS, Kale DD. Effect of succinylation on the rheological profile of starch pastes.
Carbohydrate Polymers. 2002;47:365-71.

100. Xie F, Yu L, Su B, Liu P, Wang J, Liu H, et al. Rheological properties of starches with different amylose/amylopectin ratios. Journal of Cereal Science 2009;49:371–7.

101. Fernández-Barbero A, Suárez IJ, Sierra-Martín B, Fernández-Nieves A, Nieves FJdl, Marquez M, et al. Gels and microgels for nanotechnological applications. Advances in Colloid and Interface Science. 2009;147-148:88-108.

102. Guo S, Li Y, Chen G, Li H. Ultrasonic improvement of rheological and processing behaviour of LLDPE during extrusion. Polymer International. 2003;52:68-73

103. Yadav C, Saini A, Zhang W, You X, Chauhan I, Mohanty P, et al. Plant-based nanocellulose: A review of routine and recent preparation methods with current progress in its applications as rheology modifier and 3D bioprinting. International Journal of Biological Macromolecules
2021;166:1586-616.

104. Kim MH, Lee YW, Jung W-K, Oh J, Nam SY. Enhanced rheological behaviors of alginate hydrogels with carrageenan for extrusion-based bioprinting. Mechanical Behavior of Biomedical Materials. 2019; 98:187-94.

105. Deng L, YL, LY, J-Z, FD, Li-MingZhang. Injectable and bioactive methylcellulose hydrogel carrying bone mesenchymal stem cells as a filler for critical-size defects with enhanced bone regeneration. Colloids and Surfaces B: Biointerfaces. 2020;194:111159.

106. Orasugh JT, GS, NRS, BD, AB, SD, et al. Effect of cellulose nanocrystals on the performance of drug loaded in situ gelling thermo-responsive ophthalmic formulations. International Journal of Biological Macromolecules. 2019;124:235-45.

107. Wang E, Liu Y, Xu C, Liu J. Antiproliferative and proapoptotic activities of anthocyanin and anthocyanidin extracts from blueberry fruits on B16-F10 melanoma cells. Food & Nutrition Research. 2017;61, 1325308.

108. Bhardwaj R, JB. Controlled-release delivery system for the alpha-MSH analog melanotan-I using poloxamer 407. Journal of Pharmaceutical Sciences. 1996;85(9):915-9.

109. Law N, BD, HG, YQ, ZMA, TBS, et al. Characterisation of hyaluronic acid methylcellulose hydrogels for 3D bioprinting. Journal of the Mechanical Behavior of Biomedical Materials 2018;77:389–99.

110. Wang S, JML, WYY. Smart hydrogels for 3D bioprinting. International Journal of Bioprinting. 2015;1:3-14.

111. Khoshnood N, AZ. A comprehensive review on scaffold-free bioinks for bioprinting. Bioprinting. 2020;19

VITAE

Name Wannisa Boonlai

Student ID 6110730011

Education Attainment

Degree	Name of Institution	Year of Graduation
Bachelor's degree of Science (Biology)	Thaksin University	2016
Master of Science (Drug and Cosmetics)	Walailak University	2018

Scholarship Award during Enrolment

Faculty of Pharmaceutical Sciences and Drug Delivery System Excellence Center (DDSEC), Prince of Songkla University

List of Publication and Proceeding

Boonlai W., Tantishaiyakul V., Hirun N. Characterization of K-carrageenan/ methylcellulose/cellulose nanocrystal hydrogels for 3D bioprinting. Polymer International. 2022; 71: 181–191